Nuclear Engineering and Design 444 (2025) 114412

Contents lists available at ScienceDirect

Nuclear Engineering and Design

journal homepage: www.elsevier.com/locate/nucengdes

Neutronic and thermal hydraulic analysis of ALFRED during Unprotected transients considering the reactor staged approach☆

G. Khalil Youssef [a,b], C. Ciurluini [a,*], M. Caramello [b], F. Lodi [c], F. Giannetti [a]

[a] Sapienza University of Rome, Department of Astronautical, Electrical and Energy Engineering DIAEE – Nuclear Engineering Research Group (NERG), Corso Vittorio Emanuele II, 244, 00186 Rome, Italy
[b] Ansaldo Nucleare, Via Nicola Lorenzi 8, 16152 Genova, Italy
[c] Italian National Agency for New Technologies, Energy and Sustainable Economic Development (ENEA), Via dei mille 21, 40121 Bologna, Italy

ARTICLE INFO

Keywords:
Lead fast reactors
ALFRED
Nuclear safety
Heavy liquid metals
Neutron kinetic
Thermal-hydraulics

ABSTRACT

Generation IV nuclear reactors represent the next step in nuclear technology, designed to enhance safety, sustainability, efficiency, and cost-effectiveness compared to their predecessors. These advanced reactors aim to overcome the limitations of current nuclear power systems, offering long-term energy solutions while mitigating environmental impact and improving waste management. Among the various Generation IV designs, ALFRED (Advanced Lead Fast Reactor European Demonstrator) stands out as a promising project. ALFRED is a lead-cooled fast reactor (LFR), one of the six reactor types identified by the Generation IV International Forum (GIF) as having the potential to meet the ambitious goals set for future nuclear energy systems. The reactor leverages the benefits of liquid lead as a coolant, including excellent thermal properties, a high boiling point, and inherent safety features. These characteristics allow operation at high temperatures and low pressures, reducing accident risks and enhancing overall safety. ALFRED represents a collaborative European effort under the FALCON Consortium to develop a demonstrator for lead-cooled technology, focusing on economic competitiveness and strict safety standards. While LFR technology offers significant advantages, it also introduces challenges—such as the high freezing temperature of lead (327 °C), which is particularly critical in accidental scenarios where decay heat must be removed while preventing coolant solidification. Additionally, lead's opacity complicates refuelling operations, requiring further research and development (R&D) efforts. In this context, critical R&D gaps exist in the analysis of ALFRED under unprotected transient scenarios, where limited numerical investigations are available. The complex coupling between neutronics and thermal-hydraulics in such conditions necessitates high-fidelity modelling to capture key physical phenomena that remain insufficiently explored in the literature. To address these gaps, the present work conducts detailed numerical simulations, providing valuable insights into the reactor's response under transient conditions. By leveraging advanced computational techniques, this study improves the understanding of ALFRED's safety-relevant behaviour, supporting the design and the future experimental campaigns and refining modelling strategies. For this study, three unprotected transients were selected: Unprotected Loss of Flow (ULOF), Unprotected Loss of Heat Sink (ULOHS), and Unprotected Transient Over-Power (UTOP). This paper presents the results of these scenarios, analysing ALFRED's behaviour under each condition. The transient simulations were performed using the RELAP5/Mod3.3 thermal–hydraulic system code, with a detailed description of ALFRED's nodalization scheme, transient boundary conditions, and transient evolution.

1. Introduction

The pursuit of sustainable and safe energy solutions has driven significant advancements in nuclear reactor technology. Generation IV reactors represent a major step forward, enhancing efficiency, safety, and environmental impact. Among these, the Lead-cooled Fast Reactors (LFR) stand out due to its unique features and potential benefits (GEN Iv International Forum, 2014). LFRs utilize liquid lead (Pb) as a coolant, offering advantages such as high thermal conductivity, improved

☆ This article is part of a special issue entitled: 'LFR' published in Nuclear Engineering and Design.

* Corresponding author.
E-mail address: cristiano.ciurluini@uniroma1.it (C. Ciurluini).

https://doi.org/10.1016/j.nucengdes.2025.114412
Received 2 April 2025; Received in revised form 18 August 2025; Accepted 18 August 2025
Available online 23 August 2025

Nomenclature

ALFRED	Advanced Lead-cooled Fast Reactor European Demonstrator
ANL	Argonne National Laboratory
ANS	American Nuclear Society
ANSELMUS	Advanced Nuclear Safety Evaluation of Liquid Metal Using Systems
AZ	Active Zone
BC	Boundary Condition
BoC	Begin of Cycle
BT	Bayonet Tube
CANDLE	Constant Axial shape of Neutron flux, nuclide densities, and power shape during Life of Energy production
CDF	Cumulative Damage Function
CHF	Critical Heat Flux
CR	Control Rod
CTC	Coolant Temperature Coefficient
DA	Dummy Assembly
DEC	Design Extended Conditions
DHR	Decay Heat Removal
ENEA	Agenzia nazionale per le nuove tecnologie, l'energia e lo sviluppo economico sostenibile
ENHS	Encapsulated Nuclear Heat Source
EoC	End of Cycle
FA	Fuel Assembly
FADF	Fuel Assembly Distribution Factor
FALCON	Fostering ALfred CONstruction
FPDF	Fuel Pin Distribution Factor
FTC	Fuel Temperature Coefficient
GIF	Generation IV International Forum
HP	Hot Pool
HS	Heat Structures
HTC	Heat Transfer Coefficient
HTM	Heat Transfer Mode
IC	Isolation Condenser
IS	Internal Structure
IV	Inner Vessel
LEADER	Lead-cooled European Advanced Demonstration Reactor
LFR	Lead Fast Reactor
LLNL	Lawrence Livermore National Laboratory
LP	Lower Plenum
LWR	Light Water Reactors
MYRRHA	Multi-purpose Hybrid Research Reactor for High-tech Applications
NK	Neutron Kinetic
Pb	Lead
PIE	Postulated Initiating Event
PIRT	Phenomena Identification and Ranking Table
R&D	Research and developement
RATEN ICN	Regia Autonoma Tehnologii pentru Energia Nucleara – Institutul de Cercetari Nucleare
RCP	Reactor Coolant Pump
RCS	Reactor Coolant System
RELAP	Reactor Excursion and Leak Analysis Program
RV	Reactor Vessel
RZ	Radial Zone
SD	Safety Device
SG	Steam Generator
SGTR	Steam Generator Tube Rupture
SSTAR	Small, Secure Transportable Autonomous Reactor
STC	Structural Temperature Coefficient
ULOF	Unprotected Loss of Flow
ULOHS	Unprotected Loss of Heat Sink
ULOOP	Unprotected Loss Of Off-site Power
UNIROMA1	Sapienza University of Rome
UP	Upper Plenum
URANUS	Ubiquitous, Rugged, Accident-forgiving, Nonproliferating, and Ultra-lasting Sustainer
UTOP	Unprotected Transient Over-Power

neutron economy, and enhanced safety margins due to lead's high boiling point and ability to retain fission products (Cinotti, et al., 2009). The choice of lead as a coolant enhances safety and performance, particularly when combined with mixed uranium–plutonium fuels (mainly oxides and nitrides), which allows fissile material breeding while maintaining a stable reactivity margin. The high boiling point and density of lead also eliminate the risk of positive void reactivity effects, contributing to reactor stability. Beyond neutronic advantages, the integral pool-type reactor layout limits the likelihood of coolant loss occurrences, as the probability of leaks or vessel damage is very low (International Atomic Energy Agency, 2025). Thanks to its high heat capacity, lead effectively dampens rapid temperature changes, thereby minimizing fuel damage risks in all accident scenarios excluding those involving reactivity insertions. Additionally, its density and reflectivity ensure more uniform power distribution within the core, improving performance. The benefits and potentialities related to LFR technology justify investments despite engineering challenges and cost uncertainties, holding promises for competitive deployment in the electricity market. Although, it must be reminded that the development of a First of Kind technology must also consider safety and licensing as primary aspects. Several projects worldwide are advancing LFR designs (Alemberti, et al., 2017), including the BREST-OD-300 (Orlov, 2005), an innovative fast reactor serving as a pilot for future closed fuel cycle applications. The BREST-OD-300 incorporates innovative engineering solutions for safety and efficiency, including a shroud-less hexagonal Fuel Assembly (FA) design that prevents fuel melting due to coolant blockages. This design reduces metal content by 30 % compared to conventional shrouded FAs while leveraging VVER reactor fuel assembly experience for reliability. Lead-bismuth eutectic (LBE) reactors have also been studied extensively, particularly in Europe, with MYRRHA (Baeten et al., 2014) (Bogdán, n.d) (Multi-purpose Hybrid Research Reactor for High-tech Applications) being a prominent example. MYRRHA aims to support a wide range of applications, including materials and fuel irradiation research, the testing of Generation IV reactor technologies, medical radioisotope production, and nuclear waste transmutation. MYRRHA plays a strategic role in the European roadmap for sustainable nuclear energy, particularly in demonstrating technologies for closing the nuclear fuel cycle and reducing the long-term radiotoxicity of spent nuclear fuel through partitioning and transmutation. The reactor is also expected to serve as a unique platform for international R&D in nuclear science and technology. This technology is under investigation also in Japan, where concepts like the Breed-and-Burn and CANDLE (Sekimoto, et al., 2000) (Constant Axial shape of Neutron flux, nuclide densities, and power shape during Life of Energy production) reactors were explored. These reactors offer superior neutron economy, facilitating a once-through fuel cycle (Sekimoto and Nagata, 2008). Challenges such as extreme fuel burnup conditions are addressed through metallic fuel refining processes (Sekimoto et al., 2001). Studies also investigated using plutonium from spent Light Water Reactors (LWR) fuel as an initial CANDLE core load, enhancing plutonium utilization. Research on mass transfer in LBE systems has improved understanding of iron and nickel diffusion through experiments and molecular dynamics simulations (Gao et al., 2018). Advancements in solid electrolyte oxygen sensors have enhanced stability in high-temperature LBE

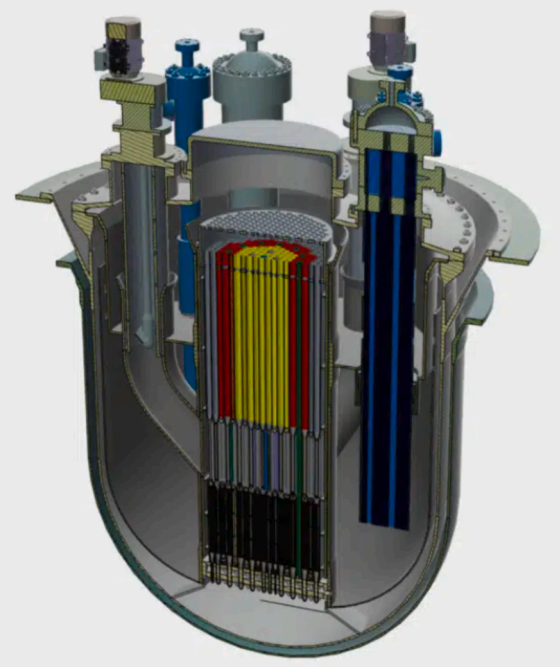

Fig. 1. ALFRED Reactor Coolant System, (Alemberti, 2020).

environments, and oxidation behaviour studies of lead-based coolants provide valuable insights for accident mitigation strategies (Martinelli et al., 2011). Work on LFR concepts in the U.S. dates back to 1997, including corrosion and thermal–hydraulic testing (Alemberti, et al., 2017). Though current U.S. LFR activities are limited, past efforts demonstrated sustained interest. The Small, Secure Transportable Autonomous Reactor (SSTAR) (Smith, 2008) by Argonne National Laboratory (ANL) and Lawrence Livermore National Laboratory (LLNL), featuring natural circulation and a long core life, exemplifies past U.S. developments. The Encapsulated Nuclear Heat Source (ENHS) (Greenspan, 2002) and a recent Westinghouse LFR initiative (Ferroni, 2022) further illustrate U.S. industry involvement. More recently, Korea has pursued LFR advancements through the PASCAR and URANUS (Choi, et al., 2011) (Ubiquitous, Rugged, Accident-forgiving, Non-proliferating, and Ultra-lasting Sustainer) concepts, focusing on safety and non-proliferation. Recent advances have focused on the development of high-fidelity numerical tools and the exploration of inherently safe core designs. For instance, in China the transient behaviour of natural circulation LFRs has been investigated through a high-fidelity multiphysics simulation framework (Dong, 2025). The study couples the OpenMOC neutron transport solver, the pin-level subchannel code KMC-FBc, and the system code RELAP5 to model the SNCLFR-100 reactor developed by the University of Science and Technology of China. The coupled tool enables accurate simulation of both steady-state and accident conditions, including unprotected transient overpower and unprotected loss of heat sink scenarios. Benchmarking against stand-alone RELAP5 calculations confirmed the reliability of the approach, which effectively captures localized thermal and neutronic behaviour in transient conditions. In parallel, recent work on the LOTUS reactor (Luo, 2022) concept has explored an innovative passive safety strategy based on the physical movement of the core during off-normal conditions. Specifically, the core is designed to passively unfold into a subcritical configuration in the event of an accident, while maintaining decay heat removal without active systems. The work focused on the development and application of a multiphysics simulation framework to analyse complex nuclear–thermal interactions during transient scenarios. The study addressed the non-linear coupling between neutron kinetics and thermal-hydraulics resulting from core deformation (Luo, 2025). Simulations were carried out using SERPENT and STAR-CCM+, combining low-dimensional neutronic evaluations with detailed coupled calculations. The results highlighted notable differences between single-physics and coupled approaches, particularly in power distribution and temperature fields, underscoring the importance of integrated modelling for accurate transient analysis in advanced reactor systems. Among the most advanced European initiatives in lead-cooled technology, the Advanced Lead Fast Reactor European Demonstrator (ALFRED) project stands out as a reference design for future demonstrators (Frignani, 2017). This innovative reactor has been developed through a collaborative effort within FALCON, a consortium of European institutions that includes ANSALDO NUCLEARE, ENEA, and RATEN ICN. ALFRED aims to demonstrate the technical feasibility and economic viability of LFRs. This project is a crucial step towards commercializing Generation IV reactors, addressing key challenges such as material corrosion, fuel cycle optimization, and passive safety mechanisms. The ALFRED reactor embodies the principles of sustainability and safety that are central to Generation IV designs. Despite progress, R&D gaps remain in coolant chemistry, structural material performance, reactor safety under transients, and fuel cycle optimization. Addressing these gaps requires systematic methodologies like Phenomena Identification and Ranking Table (PIRT) analysis (U.S. Nuclear Regulatory Commission., 1989), which prioritizes research areas characterized by high safety relevance, significant level of uncertainty in the associated physical phenomena and low modelling accuracy. For instance, a PIRT analysis was performed to support Westinghouse-LFR development (Liao, 2021). In the same way, the Advanced Nuclear Safety Evaluation of Liquid Metal Using Systems (ANSELMUS) project in Europe aims to advance safety evaluation of liquid metal-cooled reactors. ANSELMUS unites research organizations, industry experts, and academia to develop methodologies, tools, and experimental facilities for safety assessments. The project focuses on coolant chemistry, corrosion, and heat transfer phenomena, improving computational safety analysis and validation (CORDIS, n.d). A key step in European LFR development is the PIRT analysis for the ALFRED, prioritizing R&D based on EURATOM safety directive requirements. The analysis assesses knowledge gaps related to key safety parameters. For example, in the European project LEADER, a comprehensive neutronic and thermal–hydraulic studies on ALFRED's previous design has been conducted (Grasso, 2018), focusing on safety under Design Extended Conditions (DEC). The Unprotected Transient Over-Power (UTOP) and Unprotected Loss of Off-site Power (ULOOP) scenarios were identified as enveloping conditions. The UTOP case assumed a 250 pcm reactivity insertion over 10 s. This reactivity insertion value is conservatively selected in alignment with the LEADER assumptions to envelop a range of potential scenarios, including partial voiding of the active core region (regardless of the cause, such as possible void ingress among fuel pins), core compaction following the most severe yet credible earthquake, inadvertent withdrawal of the most reactive control rod, and similar events. Instead, ULOOP considered the simultaneous failure of all primary and secondary pumps. Thus, after the postulated initiating event, both the primary forced circulation and the circuit heat sink, i.e., the Steam Generators (SGs), are lost. Both scenarios excluded reactor scram to evaluate safety margins. These studies aimed to quantify potential fuel pin failure under accidental conditions. Even with conservative assumptions, no significant hazard to people or the environment was found (Grasso, 2018), reinforcing ALFRED's inherent safety. However, since ALFRED's design evolved from the LEADER project to the FALCON configuration, updated transient analyses are necessary. Design modifications impact reactor response, necessitating reassessment. Advances in computational tools further enable refined neutronic and thermal–hydraulic coupling analyses, enhancing predictive accuracy and uncertainty quantification. This ensures a more precise evaluation of ALFRED's safety performance in current configurations. This paper aims to provide a brief description of the new ALFRED design conceptualized by the FALCON consortium. It then presents the numerical model representative of ALFRED, implemented using the System Thermal-Hydraulic (STH) code RELAP5/Mod3.3

Table 1
ALFRED main parameters in the stages of operation (Alemberti, 2020).

Parameter	Unit	STAGE 0	STAGE 1	STAGE 2	STAGE 3
Core inlet temperature	°C	390	390	400	400
Core outlet temperature	°C	390	430	480	520
Core thermal power	MW	0	100	200	300
Steam line pressure	bar	/	170	175	180
Steam line temperature	°C	/	420	435	450

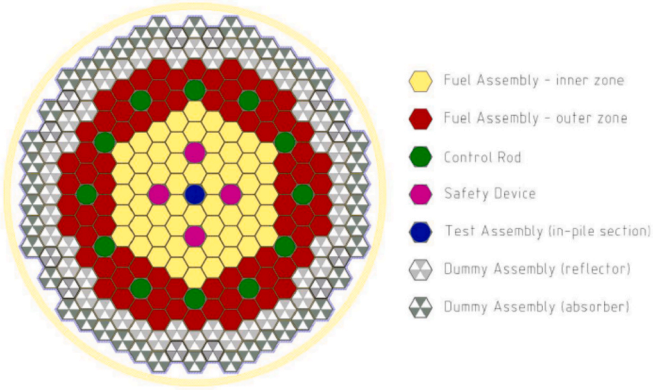

Fig. 2. ALFRED core, (Grasso, 2019).

Table 2
Power distribution factors at BoC and EoC for the two fuel zones (Grasso, 2019).

Power distribution factors	Inner zone		Outer zone	
	BoC	*EoC*	*BoC*	*EoC*
Core wise – assembly by assembly (FADF) (A)	1.292	1.162	1.154	1.164
Assembly-wise pin by pin (FPDF) (B)	1.011	1.012	1.057	1.059
Core-wise pin by pin (A*B)	1.306	1.175	1.219	1.232
Pin-wise axial (C)	1.168	1.157	1.240	1.172
Total peaking factor (A*B*C)	1.526	1.360	1.512	1.445

(Division, 2003). Since the default version of the code does not include the liquid lead among the available working fluids, a new version has been developed implementing its thermophysical properties. In addition, to assess the effectiveness of the new ALFRED design and to concurrently identify possible modelling issues, the paper focuses on the response of the reactor under three selected unprotected transients: Unprotected Loss of Flow (ULOF), Unprotected Transient Over-Power (UTOP) and Unprotected Loss of Heat Sink (ULOHS). The analysis is performed considering also the staged approach foreseen for the development of ALFRED (Frignani, 2019).

2. Overview of ALFRED design

One of the leading concepts in the development of LFR technology is ALFRED depicted in Fig. 1 (Alemberti, 2020).

Since ALFRED is an innovative reactor, a staged approach summarized in Table 1 is foreseen in order to progressively gain operating experience and face validation issues (Alemberti, 2020).

The concept involves commencing operations at low power and temperature, gradually ramping up both using the reactor itself to validate subsequent operational phases and the concurrent advancement of the R&D program. Three power levels are foreseen (100, 200, and 300 MWth), at constant primary flow rate and increasing temperature. The Reactor Coolant System (RCS) is composed of key components, including the reactor core, reactor coolant pumps (RCPs), and steam generators (SGs). While maintaining several of the main geometrical parameters of the previous core configuration (Grasso, 2014), the new design (hereafter FALCON configuration) introduces several adjustments aimed at improving neutronic and thermal–hydraulic performance and enabling in-core testing. The revised core, illustrated in Fig. 2 consists of 134 FAs (Grasso, 2019). The active region is divided into two zones: the inner and outer regions, containing 56 and 78 FAs, respectively. The inner region has MOX with an enrichment of 20.5 wt% in $PuO_{1.97}$ while the outer region is enriched to 26.2 wt%. The chosen concentrations and zoning guarantee operability in a 5-batches strategy with a criticality swing during a 1-year long equilibrium irradiation sub-cycle equal to 2200 pcm (stage 3). 126 fuel pins are arranged in a hexagonal wrapper to make up the FA (Petrovich, 2013), around a central position hosting a dummy pin for additional in-core instrumentation. FAs are surrounded by 102 Dummy Assemblies (DAs), arranged in two concentric rings. The inner ring serves to reflect leaking neutrons back into the core, while the outer ring provides radiation shielding for the inner vessel. The core central position is dedicated to in-pile irradiation experiments, allowing the testing of fuel assemblies and materials to be used in subsequent stages under neutron irradiation at temperature conditions representative of future stages.

The control and shutdown functions are ensured by 12 Control Rods (CRs) and 4 Safety Devices (SDs).

Table 2 presents the power peaking factors at the Beginning and End of an equilibrium sub-Cycle (BoC and EoC, respectively) for the newly implemented configuration. In the table, both the FA Distribution Factor (FADF) and the Fuel Pin Distribution Factor (FPDF) are reported. The former relates to the power distribution across the entire core on an assembly-by-assembly basis, while the latter details the power distribution within the hottest assembly of the inner and outer zones on a pin-by-pin level. Finally, the axial profile peak factor is also included in Table 2. The table also highlights the shift of the peak FADF from the inner to the outer zone, influenced by the partial insertion of the control rods at BoC.

The FALCON configuration also includes 3 RCPs and 3 SGs. The SGs adopt Bayonet Tubes (BTs), with an active length of 6 m, designed to interface the RCS with the secondary system. The reduction in the number of RCS components allows more space for additional auxiliary and safety systems. The passive Decay Heat Removal (DHR) system is composed of 3 loops connected to the SGs and removes decay heat from the primary coolant thanks to dedicated heat exchangers (Isolation Condensers, ICs). In the event of a loss of heat sink, the DHR system ensures that the primary coolant temperatures remain within acceptable limits. In the FALCON design, non-condensable gases are introduced to passively reduce the power removed by the DHR system (Caramello, 2017), as shown in Fig. 3.

This new configuration includes a nitrogen tank connected to the IC, improving power removal and delaying coolant freezing in the long term after a generic postulated initiating event. The system operates in a way that limits the depressurization rate, thereby delaying primary coolant freezing. It is worth to underline that the ALFRED DHR system is activated exclusively during accidental events and does not operate during normal conditions, including reactor shutdown. Additionally, an Emergency-DHR (E-DHR) system is under development to further enhance system diversity and redundancy. It would be probably used in DEC scenarios. In addition, the FALCON design foresees an Internal Structure (IS, depicted in green in Fig. 4) incorporated within the Reactor Vessel (RV) to direct the cold lead from the SG towards the lead-free level (Frignani, 2019). From there, the lead flows through openings in the IS and descends through the annular space between the IS and the RV before entering the core.

This flow arrangement prevents coolant stagnation in the upper pool region under both forced and natural circulation, mitigating thermal stratification. In the event of a Steam Generator Tube Rupture (SGTR), steam is carried along the primary flow path to the free surface and discharged into the cover gas system, preventing water ingress into the reactor core which could result in a reactivity insertion due to the water moderation and lead density variations effects. Finally, a Hot Pool (HP) has been introduced in the upper region to separate the RCPs from the

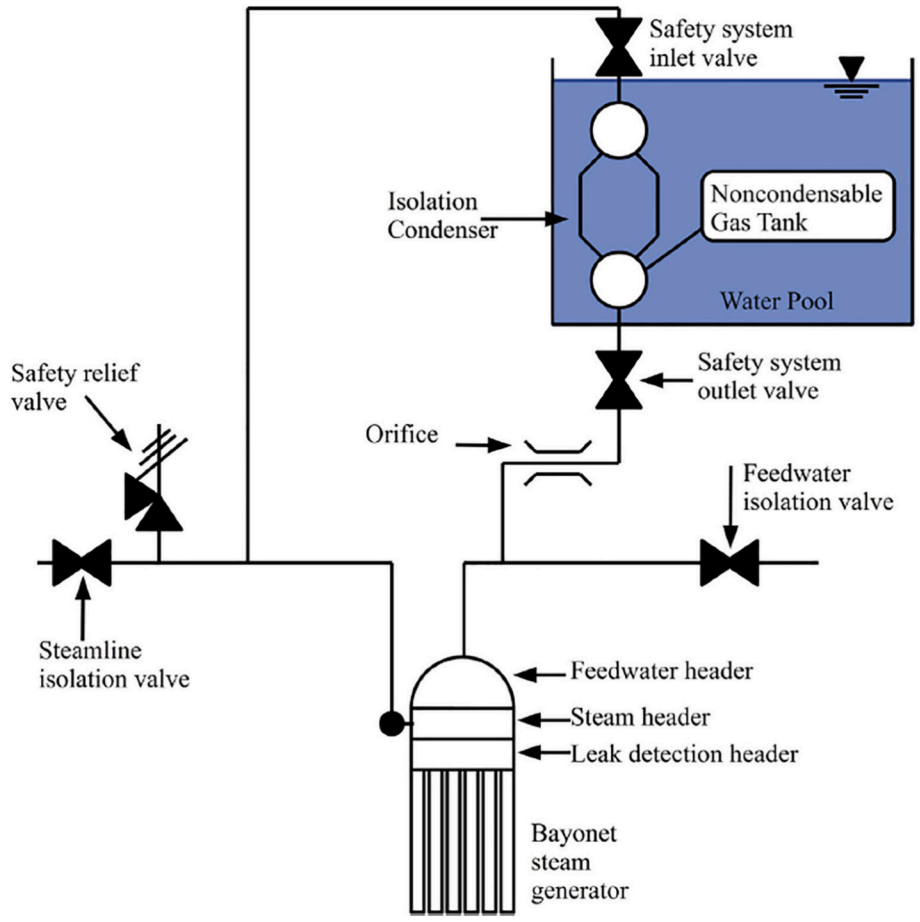

Fig. 3. DHR layout (Caramello, 2017).

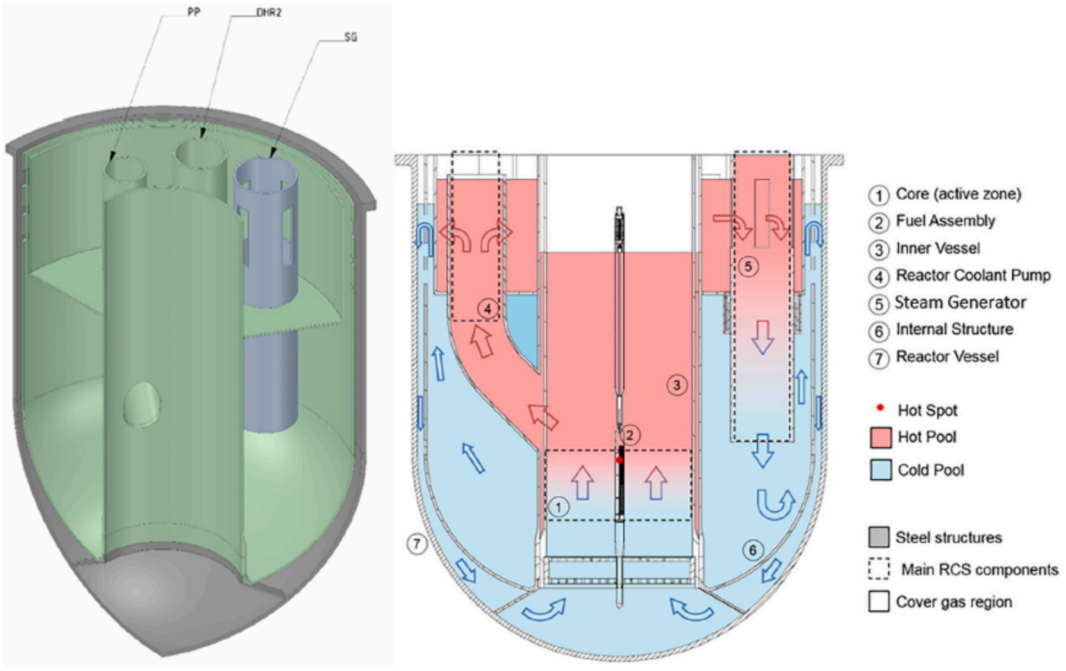

Fig. 4. Internal view of the ALFRED revised configuration and sketch of the primary flow path (Frignani, 2019).

Table 3
RPV geometry (Alemberti, 2020).

Parameter	Value	Unit
Inner diameter	8.3	m
Height	10.0	m
Vessel thickness	50	mm
Material	AISI316 LN (or L)	
Corrosion protection measure	Oxygen Control	

SGs, enhancing lead distribution at the SG inlet (Frignani, 2019). The main geometrical data of the RPV are summarised in Table 3 (Alemberti, 2020).

3. Description of the numerical model

As mentioned above, the version of RELAP5/Mod3.3 used in the present numerical activity has been suitably modified in order to include the thermophysical properties of the liquid lead (OECD/NEA Nuclear Science Committee, 2015) and the relevant heat transfer correlations (Tarantino, 2012). This modified version has been successfully applied in post-test analyses and numerical benchmark exercises (Forgione, 2019) demonstrating its reliability in capturing key phenomena observed in liquid lead experiments and providing accurate predictions of the main operating parameter trends. The numerical model is shown in Fig. 5.

Although ALFRED is a three-loops-in-pool reactor, the model

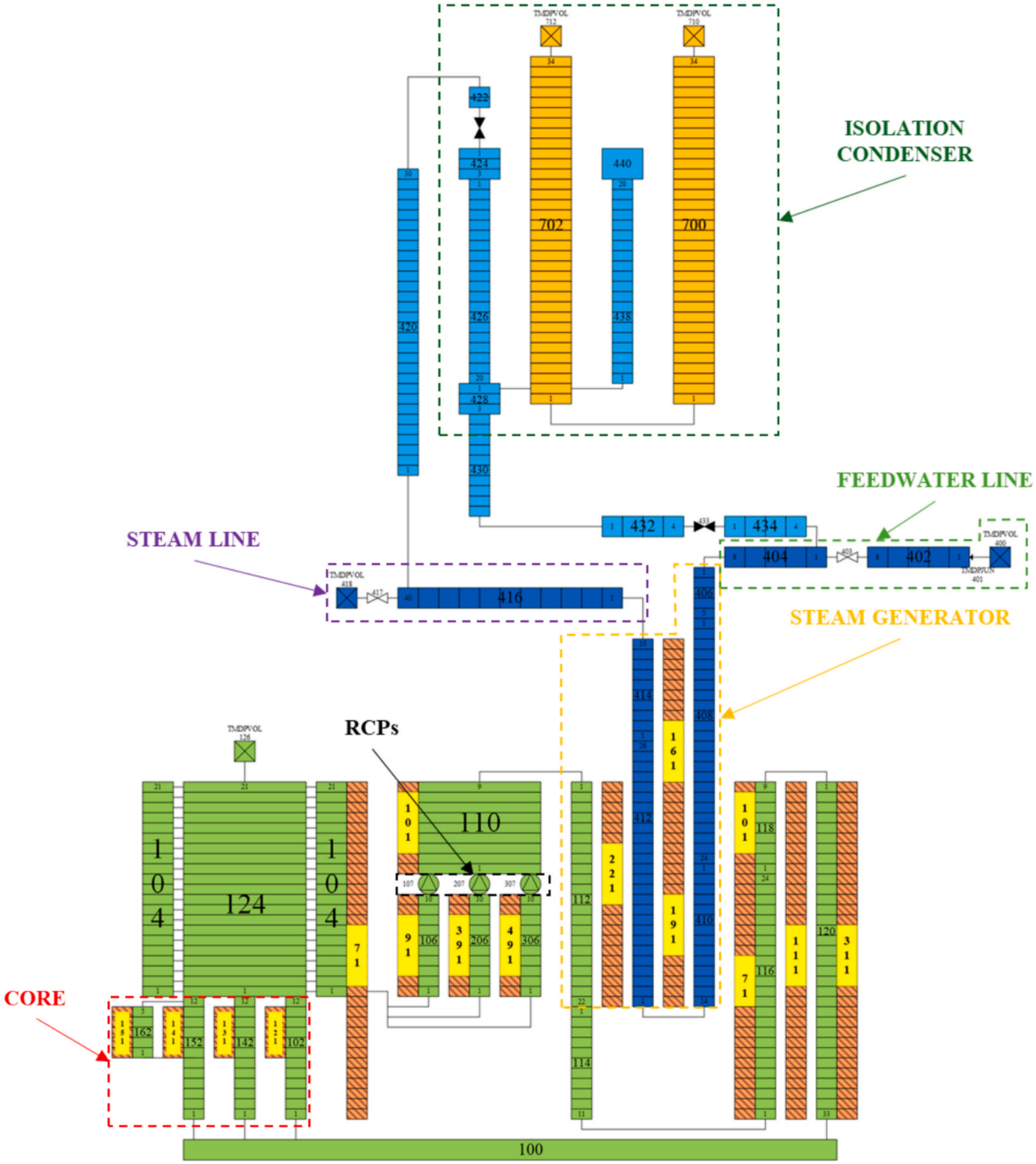

Fig. 5. R5 nodalization scheme of ALFRED.

simplifies the reactor by collapsing all three loops into a single equivalent loop, following best practices for code modelling (Laboratories, 2006). This simplification is appropriate as long as the transient under analysis does not involve asymmetric behaviour between loops, which is not the focus of this study. In Fig. 5, all control volumes coloured green represent the ALFRED reactor coolant system, while those coloured blue correspond to the in-containment section of the secondary loops, included between the isolation valves. Additionally, the numerical model includes the DHR system for ALFRED, represented by control volumes coloured cyan, with control volumes coloured orange indicating the pool side of the ICs. The first digit of the hydrodynamic components number identifies a specific system as follows:

- "1XX" for the RCS.
- "4XX" for the secondary loop and the DHR system.
- "7XX" for the pool side of the IC.

In the RELAP5 nodalization, the core is modelled with three equivalent PIPEs, numbered 102, 142 and 152. The former simulates all the reflector DAs collapsed together, while the latter two stand for the active region. PIPE 142 models the average FA behaviour, thus, represent all the core FAs minus the hottest FA collapsed together. Finally, PIPE 152 is used to assess the performance of the hottest FA. In addition, PIPE 162 has been added in parallel to PIPE 152 to simulate the subchannel interfacing with the hottest pin. From the thermal point of view, the core active Heat Structures (HS) are associated with the average FAs, the hottest FA and the hottest pin (see Fig. 5). The former two have 10 axial nodes. Among them, the actual active length is modelled with 5 nodes whose total height is 810 mm (162 mm per mesh) according to (Alemberti, 2020). Instead, the heat structure of the hottest pin models only the active length. The reactor power is distributed among these three HSs according to the radial peak factors provided in (Grasso, 2019). Furthermore, within each active HS, the power is axially distributed considering the profile provided in (Grasso, 2019). The thermophysical properties of the materials which constitute these heat structures namely the MOX fuel (International Atomic Energy Agency, 2008), the 15–15 Ti for the clad (Luzzi, 2014) and helium for the gap (Arp, et al., 1998) have been implemented in the numerical model. Given that the simulated transient involves several neutron phenomena, the Neutron-Kinetics (NK) model of RELAP has been activated. In the RELAP5 version used in this work, the only NK model available is the 0-D point model. The NK equations used by the code are the following (Division, 2003):

$$\frac{d}{dt}\varphi(t) = \frac{r(t)-\beta}{\Lambda}\varphi(t) + \sum_{i=1}^{N_d}\lambda_i C_i(t) + S \tag{1}$$

$$\frac{d}{dt}C_i(t) = \frac{\beta f_i}{\Lambda}\varphi(t) - \lambda_i C_i(t) \tag{2}$$

$$r(t) = r_o - r_B + \sum_{i=1}^{n_s} r_{si}(t) + \sum_{i=1}^{n_c} V_{ci}(t) + \sum_{i=1}^{n_\rho} a_{Wi}T_{Wi}(t) + \sum_{i=1}^{n_F} a_{Fi}T_{Fi}(t) \tag{3}$$

Where:

- t is time
- φ is the neutron flux
- C_i are the delayed neutron precursors of group i
- β is the effective delayed neutron fraction
- Λ is the prompt neutron generation time
- r is the reactivity
- f_i is the fraction of delayed neutrons of group i
- λ_i is the decay constant of group i
- S is the external neutron source
- r_o is the user-defined initial reactivity
- r_B is the bias reactivity
- r_{si} are the input tables of reactivity curves vs time
- n_s is the number of input tables
- V_{ci} are the user-defined control variables as reactivity contributions
- n_c is the number of control variables
- T_{Wi} is the volume averaged temperature of the coolant in the volume i
- a_{Wi} is the coolant temperature coefficient for the volume i
- n_ρ is the number of hydrodynamic volumes in the core
- T_{Fi} is the volume averaged temperature of the fuel in the heat structure i
- a_{Fi} is the fuel temperature coefficient for the heat structure i
- n_F is the number of heat structures in the core

The point kinetics model is used to calculate the power behaviour in a nuclear reactor by employing a space-independent approximation. This method assumes that power can be separated into spatial and temporal components, and it is suitable for scenarios where the spatial distribution of the neutron flux remains relatively constant. The adoption is justified by the nature of the transients considered, where the reactor dynamics are primarily governed by global reactivity effects and thermal–hydraulic feedback. In such cases, detailed spatial resolution of the neutron flux is not required, and the point kinetics approximation provides an adequate level of accuracy for capturing the core's global response. This approach allows for an efficient yet conservative evaluation of key safety parameters, such as temperature evolution and power excursion. The model calculates both the prompt fission power, and the power generated from the decay of fission products. The prompt power is released immediately during fission, including the energy from the kinetic motion of fission fragments and neutron moderation. Decay power, on the other hand, results from the radioactive decay of fission products and it is calculated assuming an infinite operating time using ANS94-4 data (American Nuclear Society, ANSI/ANS-5.1-, 1994) which require the fuel isotopic composition namely ^{235}U, ^{238}U, ^{239}Pu, and ^{241}Pu. The inclusion of these isotopes in the ANS 94–4 dataset makes it suitable for application to MOX fuel. However, decay heat is also strongly influenced by the neutron spectrum. ANS 94–4 is based on a thermal spectrum, while ALFRED operates with a fast spectrum. For this application, ANS itself acknowledges the limitations of the available standard curves and is considering the development of a new standard. Thus, results obtained in this work with ANS 94–4 should be refined once a more appropriate decay heat curve will be computed by using dedicated advanced numerical tools. In addition, it must be noted that a decay heat curve should be properly adopted only after an effective reactor scram. Its direct application to the point kinetics model is in line with the common practice developed for LWRs but needs further investigations, especially regarding the estimation of decay heat during operation, which is approximately 6 % of the nominal power. Eq. (1) and Eq. (2) compute the neutron population ($\varphi(t)$) and delayed neutron precursors ($C_i(t)$) and thus the generation of immediate fission power. Since the neutron population is also a function of the reactivity, this quantity ($r(t)$) can be evaluated by Eq. (3). This is the so-called separable model which defines the reactivity as the sum of separate contributions. The quantity r_o is the value given in input by the user and representing the initial reactor reactivity, usually assumed equals to zero. The quantity r_B is the bias reactivity. After input processing, it is used by the code to compensate the other contributes, the ones in Eq. (3) characterized by the summation sign and explained in the following, and to ensure that $r(t=0) = r_o$. The quantities r_{si} represent time-dependent reactivity insertions defined through a set of user-provided tables. The parameter n_s indicates the number of these tables. This approach allows the simulation of multiple reactivity insertion in the core during a transient. For example, one table may represent a sudden positive reactivity insertion, while another may simulate a negative reactivity insertion corresponding to a SCRAM curve. The V_{ci} values represent n_c control variables that can be user-defined to represent reactivity contributions, e.g., fuel axial expansion, coolant expansion, etc. $T_{Wi}(t)$ is the

Table 4
NK feedbacks implemented in the input deck.

NK Feedback	Reactivity Coeff. (pcm/K)	Ref. Temperature (description)
FTC	−0.698	Average fuel temperature within the AZ
CTC-AZ	+0.078	Average Pb temperature within the AZ
CTC-LP	−0.094	Average Pb temperature below the AZ
CTC-UP	−0.142	Average Pb temperature above the AZ
CTC-RZ	−0.080	Average Pb temperature around the AZ
STC-Clad	+0.084	Average clad temperature within the AZ
STC-Dia	−0.260	Average core inlet temperature
STC-Pads	−0.623	Average core outlet temperature
STC-CRs-IV	−0.822	IV average steel temperature between BAF and top of reactor
STC-CRs-STEM	+0.775	Average Pb temperature between BAF and top of hot pool

Table 5
ALFRED RCP main data (Alemberti, 2020).

Parameter	Value	Unit
Nominal flow rate	1908	m^3/h
Nominal head	1.5	m
Specific speed	2.97	–
Minimum/maximum flow rate	900/1980	m^3/h
Pump type	Axial/mixed flow	–
Rotational speed	289	rpm
Hydraulic efficiency	73	%
Power supply	108.15	kW
Motor supply	200	kW

spatially averaged temperature of volume i, and a_{Wi} is the temperature coefficient (excluding density effects) for volume i. The number of hydrodynamic volumes considered in the reactor core is n_ρ. This approach allows the user to compute a weighted coolant temperature coefficient based on the temperature levels in different part of the core. It is important to note that the weighting factors are included within the calculation of the a_{Wi} coefficients. The implementation of the fuel temperature coefficient is treated in a similar way. the quantity $T_{Fi}(t)$ is the average fuel temperature in heat structure i, while a_{Fi} is the corresponding fuel temperature coefficient. The number of the considered heat structures in the reactor core is n_F. The reactor physics input data required to solve the NK problem represented by Eqs. (1)–(3) have been provided by ENEA, which designed the ALFRED core (Grasso, 2019). The ERANOS code in the 2.3 N available from the Nuclear Energy Agency software database has been used for the calculations of all neutronic-related parameters along with nuclear data coming from ENDF/B-VIII.0 tapes (Brown, 2018) processed by ENEA into an ERANOS-readable format (Castelluccio, 2022). The computed parameters are the delayed neutron fraction (β), the delayed neutron yield ratio for each group (f_i, six groups are considered), the delayed neutron decay constant for each group (λ_i) and prompt neutron generation time (Λ). Since no neutron sources are present in the reactor, the 'S' term in Eq. (1) can be neglected. For the ALFRED transient analysis, several NK feedbacks have also been considered in the input deck. The Fuel Temperature Coefficient (FTC), which comprises the Doppler effect and the fuel expansion, and the Coolant Temperature (i.e., density) Coefficient associated with the Active Zone (CTC-AZ) have been implemented by using the approach considering a_{Wi} and a_{Fi} coefficients. The hydrodynamic volumes and heat structures related to the core active zone (see Fig. 5) have been accounted for. Instead, the coolant temperature coefficient referred to the upper plenum (CTC-UP), lower plenum (CTC-LP) and Radial Zone (CTC-RZ) around the active region have been introduced by means of control variables (V_{ci}). The same methodology has been adopted for the Structural Temperature Coefficients, accounting for the metallic structures within the active zone (STC-Clad), the diagrid (STC-Dia), the expansion pads (STC-Pads), and the control and safety rods (STC-CRs). The latter consists of two different contributions. Considering that CRs and SRs enter the core from the bottom, during heating transients, when the stems that hold these components in position axially expand, the CRs and SRs are gradually extracted from the core, resulting in positive reactivity feedback (labelled STC-CRs-STEM). What effectively rules this feedback is the axial temperature profile of the stem going approximately from the Bottom of Active Fuel (BAF) to the top of the hot pool. Considering the low mass and volume of the stem, in the current simplified NK model based on nodal kinetics, its inertia is neglected, and the average coolant temperature is computed in this axial region and adopted as controlling parameter for this reactivity feedback. In addition, it must be considered that the core is supported by the lower support plate anchored to the Inner Vessel (IV see Fig. 4). During heating transients, when the IV axially expands in the downwards direction, it carries with it also the support plate and the core leaning over. Since the CRs and SRs are hanging from above, they do not move with the rest of the core structure. In conclusion, the downwards displacement of the core produces an insertion of the CRs/SRs, resulting in negative reactivity feedback (labelled STC-CRs-IV). Also in this case, it is the axial temperature profile associated with the IV steel structure that rules the reactivity feedback (from approximately BAF to top of reactor). For this, the related average temperature is computed and used as controlling parameter. The logic associated with the implemented control variables, is shown below:

$$V_{ci}(t) = a_i(T_i - T_{0i}) \tag{4}$$

It corresponds to a linear reactivity variation as function of the temperature difference with respect to a nominal value (T_{0i}). Eq. *(4)* is implemented by using a table, centred at the steady state conditions corresponding to the desired power level, to have null feedback in those conditions. For each NK feedback, the a_i coefficient in Eq. (4) is shown in Table 4. The feedback coefficients were computed with ERANOS combining the pertinent feedback effects as described in (Grasso, 2018). The feedback effects have been calculated via variations to the reference parameters (taken in their STAGE 3 value), meaning fuel temperature, lead density in various regions of the system, steel density, fuel density, active height, absorber height and FA pitch exactly as in (Grasso, 2018).

Finally, an important aspect to be highlighted is that the NK feedback associated with the pads radial expansion is a threshold effect. This means that if the core outlet temperature is below a critical value, this reactivity feedback is neglected. For sake of clarity, the implemented logic is reported in Eq. (5):

$$\begin{cases} T_{Pboutcore} \le T_{crit} \rightarrow \Delta\rho_{Pads} = 0 \\ T_{Pboutcore} > T_{crit} \rightarrow \Delta\rho_{Pads} = a_i(T_{Pboutcore} - T_{Pboutcore,ref}) \\ T_{crit} = 520 + 0.977^*(T_{Pbincore} - 400) \end{cases} \tag{5}$$

This logic was selected to properly simulate the pads NK effect. These components consist in outward protrusions machined on the FAs wrapper tube. They are designed to enter in contact when the core works in STAGE 3 nominal conditions. Indeed, retrieving the STAGE 3 data from Table 1, it is possible to see that, if core inlet temperature coincides with the nominal value, the critical temperature (T_{crit}) approaches the nominal core outlet temperature and the pads NK feedback ($\Delta\rho_{Pads}$) is equals to zero. When the core outlet temperature exceeds the nominal value, the pads radially expand provoking an increase of the core radius and of the coolant volume fraction (at the expenses of the fuel one), i.e., negative reactivity feedback. However, to properly account for this phenomenon, the pads radial expansion must be compared with the one occurring at the core bottom and due to the diagrid, caused by an increase in the core inlet temperature. It is the relative radial expansion of the pads with respect to the diagrid that actually rules FA outwards flowering and thus this NK feedback. For this a threshold is inserted in Eq. (5) and this threshold is proportional to the core inlet temperature increase with respect to its nominal value.

The ALFRED primary system model comprises three pumps, three

Table 6
STAGE 2 full power calculations: steady state results.

Parameter	Unit	Nominal Data (Alemberti, 2020)	RELAP5 result	Deviation
Thermal power (BC)	MW	200	200	/
Total lead mass flow rate	kg/s	16845.6	17218.2	+2.2 %
Core inlet temperature	°C	400	400.0	0 °C
Average core outlet temperature	°C	480	480.0	0° C
II SG inlet temperature (BC)	°C	335	335	/
II SG outlet temperature	°C	435	431.8	−3.2 °C
II SG pressure (BC)	bar	175	175	/
II SG mass flow rate	kg/s	132.9	133.7	+0.6 %
Max. Fuel temperature	°C	–	1402.4	/
Max. Clad temperature	°C	–	500.9	/

Table 7
STAGE 3 full power calculations: steady state results.

Parameter	Unit	Nominal Data (Alemberti, 2020)	RELAP5 result	Deviation
Thermal power (BC)	MW	300	300	/
Total lead mass flow rate	kg/s	16845.6	17268.9	2.5 %
Core inlet temperature	°C	400	400.0	0 °C
Average core outlet temperature	°C	520	520.0	0 °C
II SG inlet temperature (BC)	°C	335	335	/
II SG outlet temperature	°C	450	449.0	−1.0 °C
II SG pressure (BC)	bar	180	180	/
II SG mass flow rate	kg/s	192.5	193.4	0.5 %
Max. Fuel temperature	°C	–	1954.5	/
Max. Clad temperature	°C	–	550.9	/

SGs and several PIPE components that simulate the lead volumes within the RV, as shown in Fig. 4.

The three RCPs are simulated with RELAP5 PUMP components. The component nominal data, as well as homologous curves have been implemented according to the information provided by ANSALDO. The main parameters of the ALFRED RCP implemented in the RELAP5 component are shown in Table 5 (Alemberti, 2020).

Several passive HSs have been introduced in the input deck to simulate the main steel structures present in the reactor layout. HS 71 represents the IV. HSs 91, 391 and 491 model the pump ducts. HSs 101 and 111 represent the IS and finally HS 311 simulates the RV (see Fig. 4). These HSs are fundamental to properly model the reactor thermal inertia during transient conditions.

On the other hand, in the secondary loop, the feed water flow is simulated by the TMDPVOL 400 which imposes the pressure and temperature conditions at the SG inlet, and by the TMDPJUN 401 which imposes the desired feed water mass flow rate. The feedwater enters the SG and exits as superheated steam which then moves toward the turbines represented by the TMDPVOL 418. The bayonet tube SG is modelled as follows: PIPE 406 and PIPE 414 represent the feedwater and steam headers, respectively; PIPE 408 and PIPE 410 simulate the tubes downcomer section, where the regenerative heat transfer with the riser section occurs. Finally, the riser of the SG tube bundle is modelled by PIPE 412 which is thermally coupled with the liquid lead that flows in the SG shell side represented by PIPE 112. Primary and secondary sides are thermally coupled by means of HS 221 (see Fig. 5). Additionally, the HS 161 and HS 191 models the regenerative heat transfer between the riser and the downcomer.

The thermal properties for the bayonet tube steel (i.e., AISI316L) are derived from (Kim, n.d). The heat transfer coefficient in the lead side is evaluated by Mikityuk correlation (Mikityuk, 2009) suitable for fuel and tube bundles. In the SG secondary side, water experiences the phase transition from subcooled liquid up to superheated steam. In RELAP5, the correlation used to assess the Heat Transfer Coefficient (HTC) depends on the predicted Heat Transfer Mode (HTM) (Nuclear and Commission, 2006). For subcooled fluid and when the wall temperature is below the saturation temperature at the fluid total pressure, single-phase liquid convection is predicted, and Dittus-Boelter correlation is adopted (Dittus and Boelter, 1930). If fluid flows outside a tube bundle, the enhanced turbulence is accounted by multiplying the previous with the turbulent flow corrective factor developed by Inayatov (Inayatov, 1975) and based on the tube pitch-to-tube diameter ratio. When the wall temperature exceeds the saturation temperature at the fluid total pressure, nucleate boiling starts on the tube outer surface. In this case, RELAP5 uses the Chen correlation (Chen, 1966). When a significant amount of water is vaporized, the liquid layer on the tube outer surface is replaced with a steam blanket, hindering the heat transfer due to the insulating effect of the vapor layer (dry-out). The corresponding heat flux is called Critical Heat Flux (CHF). When CHF occurs, the HTM shifts to Film Boiling. To evaluate the CHF, RELAP5 uses the 1986 Groeneveld Look-Up Tables (Groeneveld, 1986). In the post-dry-out region, the system code evaluates the HTC as the maximum between two different correlations: the Chen transition boiling model, (Chen et al., 1977), and the Bromley film boiling model corrected by Sudo, (Bromley, 1950) (Sudo, 1980). Finally, when the fluid void fraction exceeds 0.999, RELAP5 switches to single-phase vapor convection and assess the HTC as for the single-phase liquid convection.

For the primary and secondary loops, from the hydraulic point of

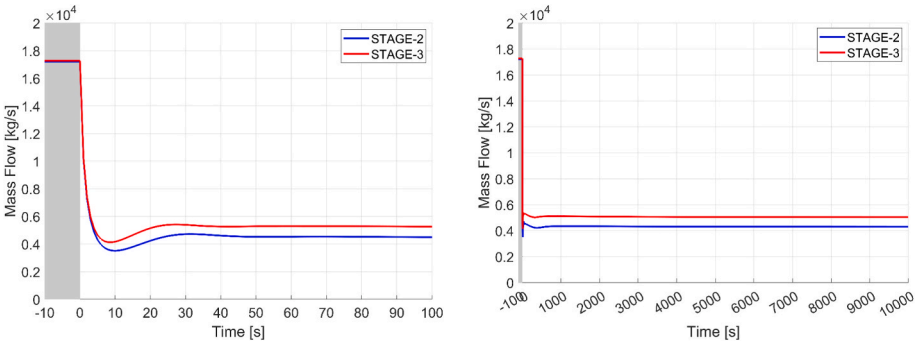

Fig. 6. ULOF transient: RCS mass flow rate in short-term (left) and long-term (right).

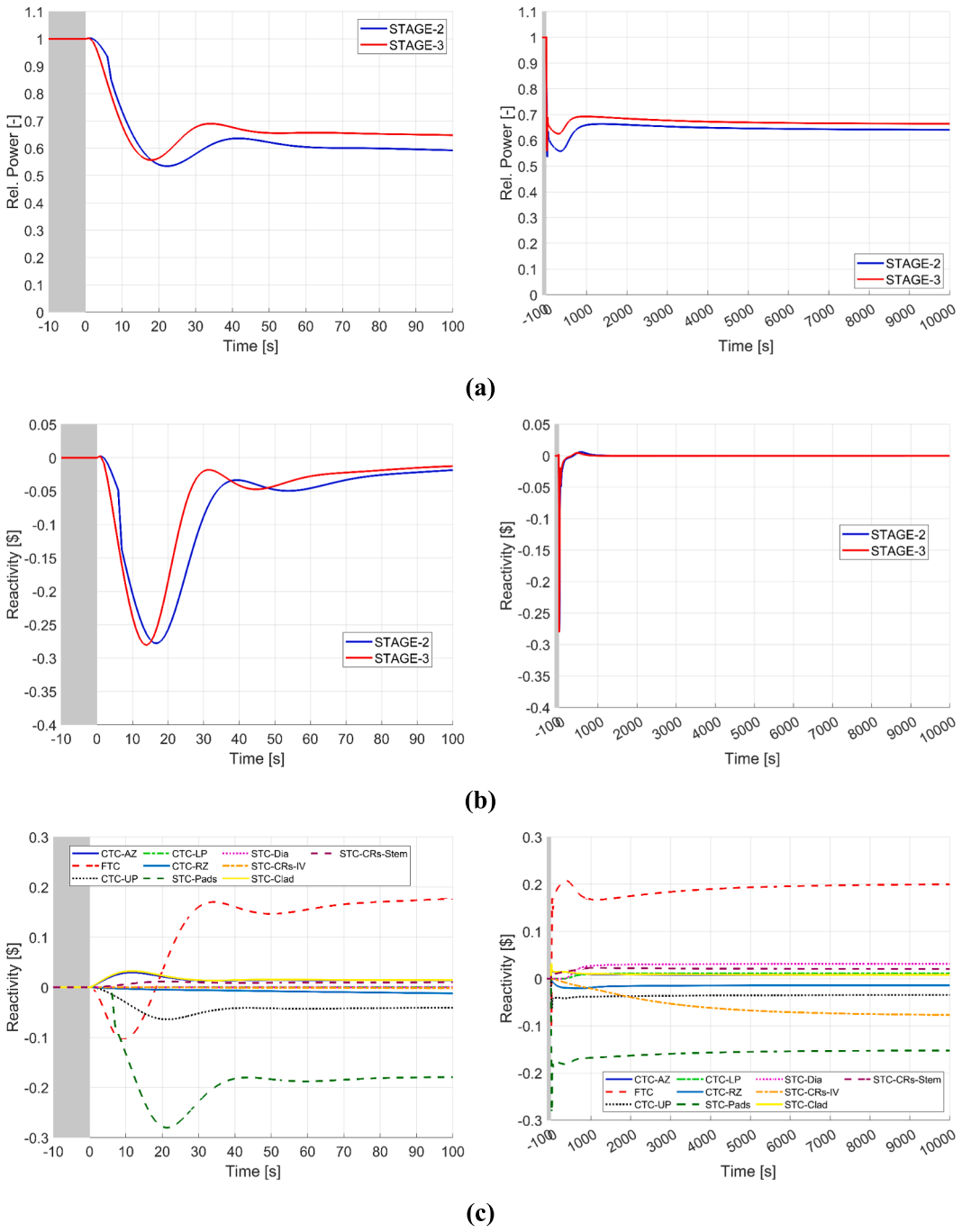

Fig. 7. ULOF transient: relative reactor power (a), total reactivity (b), STAGE 2 (c) and STAGE 3 (d) NK feedbacks, in short-term (left) and long-term (right).

view, the friction factor associated with the distributed pressure drops is computed by Colebrook correlation (Colebrook and White, 1937), that is the default one in RELAP5. In the SG secondary side, where two-phase mixture is present, the Lockhart-Martinelli multiplier is also considered (Lockhart and Martinelli, 1949). Instead, the K-loss coefficients related to concentrated head losses must be given in input by the user. They have been evaluated according to the formulas indicated in the Idelchik hydraulic handbook (Idelchik, 1986). In addition, concentrated pressure drops at the bottom of PIPEs 142, 152 and 162, have been used to simulate the FA inlet orifice. They have been tuned to obtain the proper core gagging scheme. The goal is to keep the maximum clad temperature below the limit indicated in (Bandini and Polidori, 2013). Clearly, the reference scenario is STAGE 3, where the core temperature level is higher (see Table 1). Finally, the three RCPs on the primary system and the TMDPJUN 401 on the secondary loop are provided with an integral control system given by Eq. (6) Eq. (7) to regulate the pump velocity in the primary loop and the mass flow rate of the secondary side respectively:

$$\Delta\omega = K_I \int_0^t e(\tau)d\tau \tag{6}$$

$$\Delta\Gamma = K_I \int_0^t e(\tau)d\tau \tag{7}$$

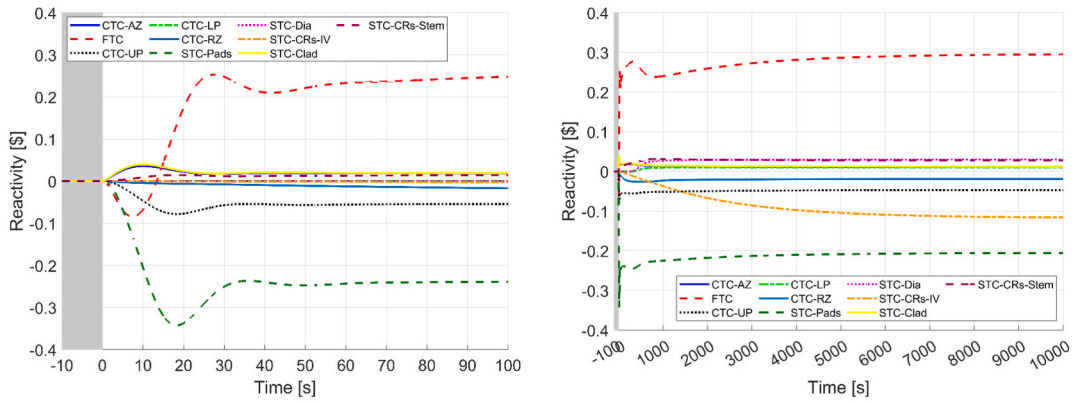

(d)

Fig. 7. (*continued*).

In which:

- $\Delta\omega$ is the primary pump velocity variation
- $\Delta\Gamma$ is the secondary (feedwater) mass flow rate variation
- K_I is the integral constant
- $e(\tau)$ is the error based on a setpoint

The integral controllers were used during the steady state calculations to obtain the nominal reactor parameters, according to indications provided in Table 1 (Alemberti, 2020). The setpoints of the RCPs and the TMDPJUN 401 with which the errors are computed are the core outlet and inlet temperatures, respectively. In this way, the primary loop thermal cycle is correctly reproduced for each reactor operational stage that is simulated. The integral controllers were selected (with respect to other controller options, i.e., proportional, derivative or combination of them) since, even if with higher computational times, they tend to the given setpoint with smoother trends, avoiding oscillations around the desired value and ensuring the stability of the numerical solution obtained. Finally, it is worth to be mentioned that the heat losses were not explicitly modelled over the entire numerical model of ALFRED reactor. This is a conservative assumption for the transient analysis since one heat sink of the primary system is neglected (even if it represents a minor aspect). Indeed, given the reactor layout, the vessel insulation thickness can be sized such that heat losses remain negligible compared to the reactor power, while remaining consistent with acceptable insulation costs. As such, this is a design-related aspect that does not jeopardize the transient results obtained and discussed in this paper.

4. Numerical analysis

This numerical activity started from steady state numerical simulations that represent the normal operation of ALFRED both at STAGE 2 and STAGE 3. At STAGE 2, the core produces a fission power of 200 MW, which is removed by a liquid lead coolant flow rate of approximately 17000 kg/s. The coolant enters the core at 400 °C and exits at 480 °C. The thermal power is then transferred to the secondary loop through the steam generators. In the secondary loop, this power is removed by a water flow rate of around 133 kg/s, with the fluid entering at 335 °C and exiting at 435 °C. During STAGE 2, the secondary loop operates at a pressure of 175 bar. Table 6 summarizes the key results of the full power steady state calculation. Parameters indicated with '(BC)' are the ones imposed as boundary conditions for the current calculation. In Table 6, a slight deviation worth to be discussed is the one associated with the primary mass flow. As discussed in section 3, the core inlet temperature is set to the nominal value by adjusting the SG secondary feedwater flow. In addition, the primary pump speed is regulated to obtain the nominal core outlet temperature. Indeed, for both these parameters, the associated error is negligible in Table 6. Given the core power, that is imposed as BC, and the correct inlet/outlet temperatures, for the core power balance, the only possible source of deviation in the primary mass flow evaluation are the liquid metal thermophysical properties, e.g., the lead heat capacity. This is because the empirical correlations used in RELAP5 (OECD/NEA Nuclear Science Committee, 2015), are slightly different from the ones used to calculate the parameters in Table 1. Finally, another small deviation can be detected in the SG secondary feedwater flow and, consequently in the steam outlet temperature. Indeed, the former is a little higher than its nominal value and, accordingly, the latter a bit lower (i.e., the thermal power exchanged by the SG is the nominal one). This is related to the fact that RELAP5 slightly underestimates the heat transfer within the component. Thus, to exchange the SG nominal power, the control system must increase the feedwater flow. However, the discrepancy is very limited (0.5 %). If it seems higher when it comes to steam outlet temperature is only because, for superheated steam, the temperature is very sensitive with the fluid enthalpy. Thus, even a small difference in the latter causes a higher deviation in the former (of the order of some degrees).

On the other hand, at STAGE 3, the core produces a fission power of 300 MW. Primary mass flow is the same of STAGE 2. The coolant enters the core at 400 °C and exits at 520 °C. In the steam generators, the thermal power is removed by a water flow rate of around 192 kg/s, with the fluid entering at 335 °C and exiting at 450 °C. During STAGE 3, the secondary loop operates at a pressure of 180 bar. Table 7 summarizes the key results of the full power steady state calculation. Here, the same slight deviation of Table 6 related to the liquid lead mass flow can be detected. As expected, passing from STAGE 2 to STAGE 3, clad and fuel maximum temperatures increase significantly. It should be noted that, for both stages, the maximum clad temperature associated with the heat structure simulating the hottest pin (i.e., HS 151 in Fig. 5) is below or equals to the limit value indicated for this parameter during normal operations in (Bandini and Polidori, 2013). This has been obtained by increasing the flow rate through the subchannel that interfaces with this heat structure (i.e., PIPE 162 in Fig. 5). By design, the average mass flow cooling each pin is nearly 1 kg/s (compare data in section 2 and in Table 7). Instead, according to simulation results, a mass flow of about 130 % of the average value is needed in STAGE 3 to keep the clad maximum temperature below the limit. To reach this goal, the concentrated pressure drops at the inlet of PIPEs 142, 152 and 162, simulating the FA inlet orifice, have been accordingly tuned. However, this has been done by preserving the total core pressure drops that have been aligned to the design value of 1 bar, indicated in (Bandini and Polidori, 2013).

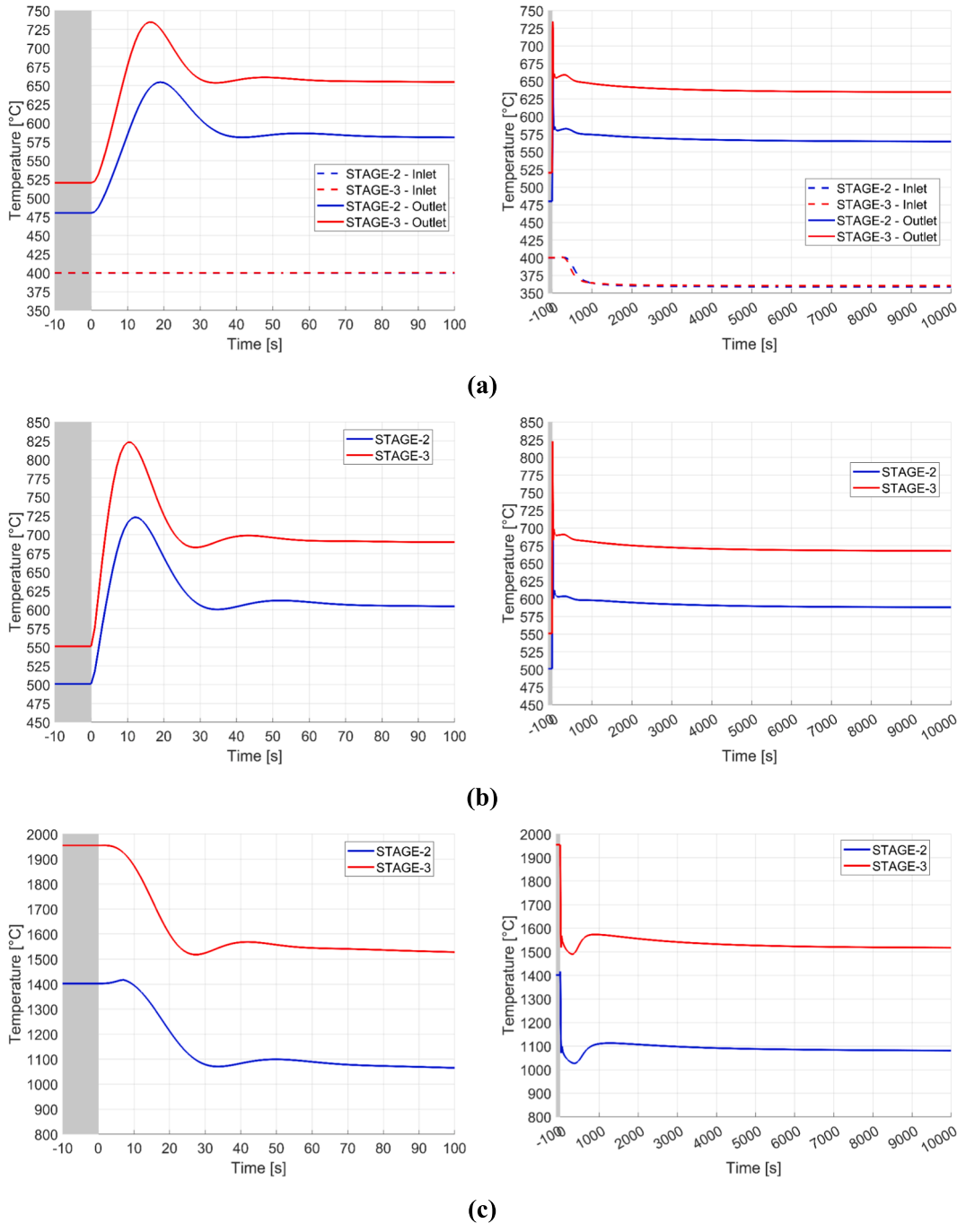

Fig. 8. ULOF transient: core inlet/outlet temperatures (a), maximum clad temperature (b) maximum fuel temperature (c), in short-term (left) and long-term (right).

4.1. Description of selected unprotected transients

Starting from these ALFRED steady state calculations, the analysis of DEC transients has been performed. The safety analysis follows a deterministic approach, employing a methodology similar to that used for LWRs (Samanta, et al., 2019); namely, evaluating the consequences of selected Postulated Initiating Events (PIEs) that could occur in the ALFRED reactor. Three accidental transients were investigated with the aim to understand the reactor behaviour under abnormal conditions. The selected PIEs are: Loss of Flow (section 4.2); Over-Power Transient (section 4.3); Loss Of Heat Sink (section 4.4). These scenarios were primarily studied to gain insight into the intrinsic safety features of ALFRED and to preliminarily assess the adequacy of the core and plant design solutions. In all three cases, the postulated DEC includes the failure of the reactor SCRAM, leading to unprotected transients. Additionally, the failure of the DHR system was also assumed as an aggravating condition. In the ULOF scenario, the transient involves the loss of core coolant flow due to failure of the RCPs, caused by a loss of their electrical power supply. However, the secondary loop is assumed to remain in normal operation, with the feedwater mass flow rate kept constant at its nominal value. In the UTOP case, a reactivity insertion of 250 pcm within 10 s is assumed. This insertion is intended to conservatively envelop the effects of potential voiding in part of the active core region—regardless of the cause, including SGTR, core compaction, FA blockage, etc.—in line with the assumptions in (Bandini and Polidori, 2013). The primary and secondary loops are assumed to remain in normal operation, i.e., the forced circulation is kept in both systems. For the ULOHS scenario, the loss of feedwater to the SGs is postulated. In this

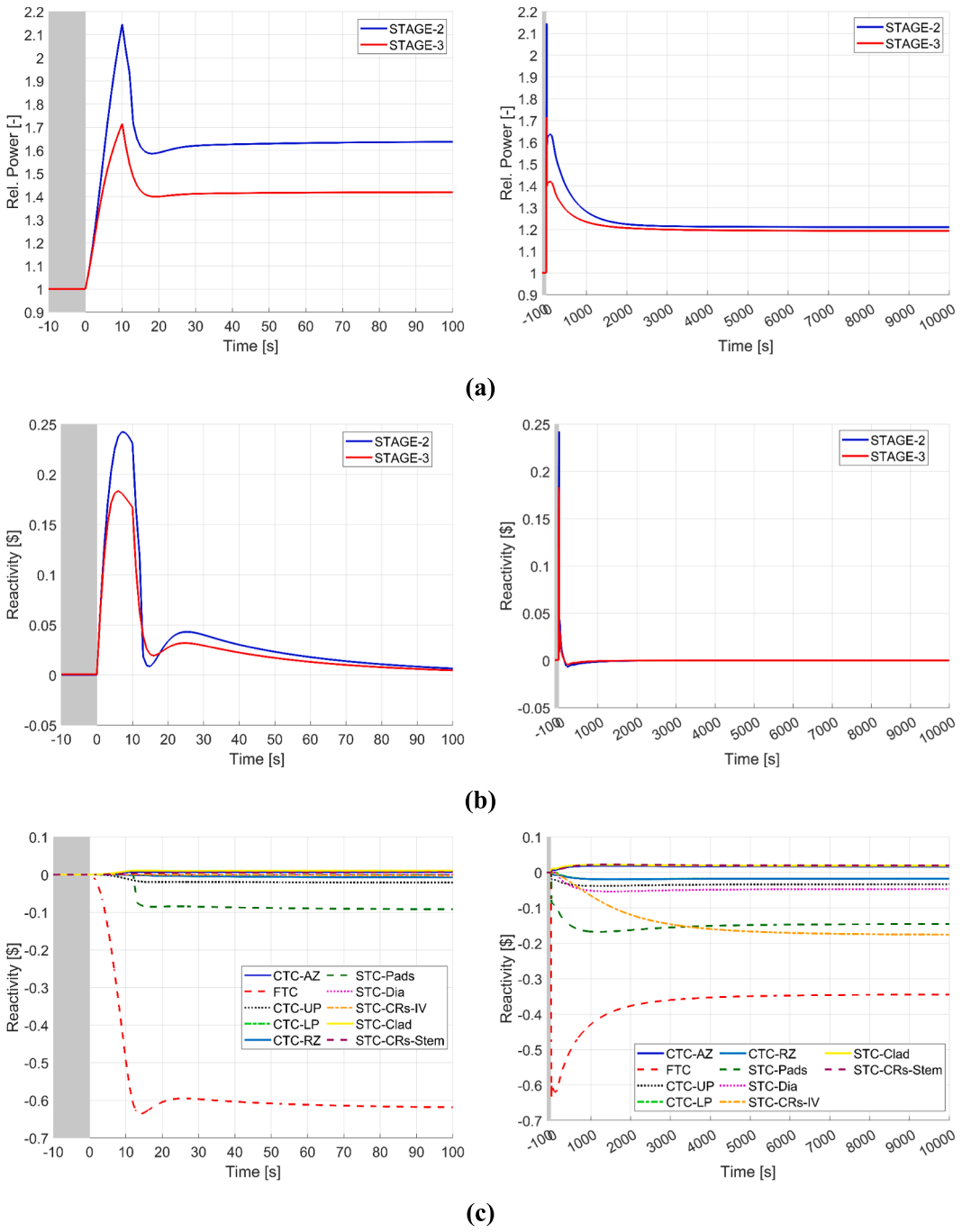

Fig. 9. UTOP transient: relative reactor power (a), total reactivity (b), STAGE 2 (c) and STAGE 3 (d) NK feedbacks, in short-term (left) and long-term (right).

case, forced circulation in the primary system is maintained. In all the considered scenarios, the integrity of the fuel pellet and the clad were preliminary verified. As far as the fuel is concerned, its corresponding maximum temperature was monitored during all the transient evolutions and compared with its relative melting temperatures which is 2800 °C according to its isotopic composition (Topliss, 1995). With regard to the clad, its maximum temperature was monitored and compared to its melting temperature which is 1417 °C (Luzzi, 2014). In addition, its creep resistance can be preliminarily evaluated with the correlation provided in (Lodi and Grasso, 2018) and reported in Eq. (8), even though additional dedicated mechanical calculations should be performed to ensure the absence of other failure phenomena.

$$t_{failure} = 10^{\frac{1520-\sigma_{eff}}{0.086T}-13} \tag{8}$$

In the previous, σ_{eff} is the effective stress in the cladding expressed in MPa, T is the clad temperature expressed in K and $t_{failure}$ is the time-to failure expressed in hours. A first-tentative value for the σ_{eff} was calculated in (Lodi and Grasso, 2018) using TEMIDE (Lodi, 2018) and it was used in the current work. It corresponds to 36 MPa. In accordance with (Lodi and Grasso, 2018), this preliminary σ_{eff} value is independent from the maximum cladding temperature. However, in the future development of the activity, a more valuable estimation of this parameter will be obtained by performing a dedicated thermomechanical analysis.

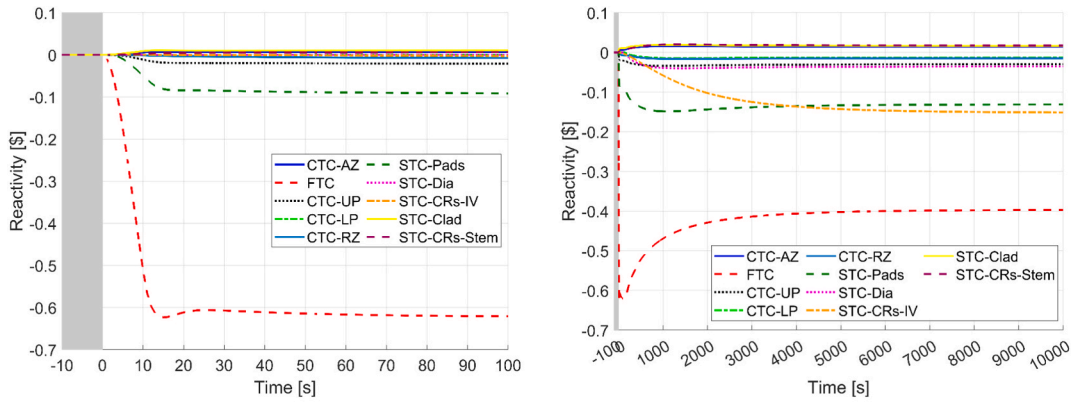

(d)

Fig. 9. (*continued*).

4.2. Unprotected loss of flow

The PIE associated with this scenario is the loss of power supply to all primary pumps. Both the reactor SCRAM and the ALFRED DHR are supposed to fail. Instead, the secondary loop is assumed to operate in normal operation with no control of the feedwater mass flow rate. After the PIE, the RCPs decelerate according to the torque-inertia equation and the component moment of inertia. In the mid-long term, they become an additional concentrated head loss along the liquid lead primary flow path. The extent of this pressure drop is consistent with the homologous curves provided by ANSALDO. After the RCPs coast down, the natural circulation establishes in the primary loop. As visible in Fig. 6, the mass flow trend is independent from the initial reactor stage since the pump component is the same and the mass flow rate in steady-state conditions is the same. However, in case of STAGE 3, the new steady state value is higher (29 % vs 25 % of nominal value, see Table 6 and Table 7) due to the increased average temperature level in the primary circuit.

The relative reactor power trends are shown in Fig. 7a. From the figure, it can be seen that in the short-term, for both stages the power decreases rapidly to 50 % of nominal power, with a slightly faster slope for STAGE 3. This is because the reactivity in STAGE 3 reduces earlier than in STAGE 2, due to the threshold behaviour of the STC-Pads: in STAGE 3, they provide a non-zero feedback immediately after the PIE, whereas in STAGE 2, the pads take approximately 5 s to reach the temperature threshold and give a non-zero feedback. Then for both stages, the reactor power stabilizes nearly at 65 % of the nominal power. The power trend is consistent with the one of the total reactivity (Fig. 7b), where, after the perturbation following the PIE, the zero value is restored after about 25 min (i.e., 1500 s). Even more information can be deduced by the NK feedbacks reported in Fig. 7c and Fig. 7d, for STAGE 2 and STAGE 3 respectively. To understand these figures, the acronyms defined in section 3 must be recalled. In the short term, as expected, the NK feedbacks provoking the sharp power decrease is the FTC and STC-Pads (red and dark green dashed lines in Fig. 7c and Fig. 7d). Indeed, the pad system has been designed to quickly intervene in overtemperature transients to radially expand the core and, consequently, to introduce negative reactivity feedback (i.e., smoothing the power peak). In the mid-term (i.e., hundreds of seconds), the FTC changes sign and becomes positive due to the drop of the fuel temperature. Nevertheless, this contribution is overcome by the negative reactivity feedbacks due to coolant density coefficient in the upper plenum and the radial expansion of the core pads. For this, the reactor power keeps decreasing. In fact, in this time scale, the temperature change can be only detected in the core itself and at the core outlet (i.e., upper plenum). After nearly 400 s, the lower plenum and, thus, the core inlet, is reached by the colder fluid coming from the steam generators. Indeed, within these components, the drop of the lead mass flow, produces a consequent decrease of the SG primary outlet temperature (i.e., the primary temperature difference increases). This triggers the positive NK feedback associated with the diagrid contraction (pink dotted line in Fig. 7c and Fig. 7d). In addition, in the long term (i.e., thousands of seconds), temperature effects become also detectable in the reactor hot pool and IV. Thus, they are also visible related to the CRs feedbacks, positive for STC-CRs-STEM (magenta dashed/dotted line) and negative for STC-CRs-IV (orange dashed/dotted line), as discussed in section 3. Together with the FTC, they restore the equilibrium, leading the total reactivity to zero. The NK transient is very similar when considering both STAGE 2 and STAGE 3. The only slight deviation is visible in the short-mid-term, and it is due to the timing needed to the cold lead exiting the steam generator to propagate up to the lower plenum and, thus, the core inlet, producing the positive NK feedback associated with the diagrid contraction. The power-to-mass ratio differs in the two cases, leading to a different thermal inertia of the system when withstanding this accidental scenario. In STAGE 2, this ratio is lower and, thus, the reactor thermal inertia is higher. This smooths the main transient oscillations visible in the power trend in both the short (between 20 and 40 s) and mid-term (up to 400 s). After, the cold lead reaches the lower plenum, the transient proceeds in a common way in both the calculations. From this moment onwards, the effect of the thermal inertia is negligible.

Fig. 8a shows the core inlet (dashed lines) and outlet (solid lines) temperatures for STAGE 2 (blue lines) and STAGE 3 (red lines). As already pointed out, the inlet temperature reduces only in the long-term. This is due to the reduction in the primary system mass flow and the degradation of the SGs heat transfer performance. On the other hand, the core coolant outlet temperature increases after PIE due to the mismatch between the generated thermal power and the core flow rate. The short-term peak for STAGE 2 and STAGE 3 corresponds to 655 °C and 735 °C, i.e., 136 % and 141 % of the nominal value (Table 6 and Table 7). The final value of the core inlet temperature for both stages are approximately 360 °C, while the outlet temperatures are 565 °C and 635 °C respectively for STAGE 2 and STAGE 3, i.e., 118 and 122 % of the nominal values in Table 6 and Table 7. Particular attention must be paid to the primary system minimum temperature. Due to the absence of dedicated modelling for heat losses, the evaluation of the freezing margin is limited. Nonetheless, this aspect is considered of secondary importance in the context of the present transient scenario. Apart from the previous issue, coolant core inlet and outlet temperatures are not strictly related to any safety criteria, but they are useful to quickly understand in a quantitative way the deviation of the primary fluid system from the nominal state occurring after the PIE. Fig. 8b shows the trend of the maximum clad temperature where a sudden increase occurs due to the failure to remove the thermal power caused by the interruption of

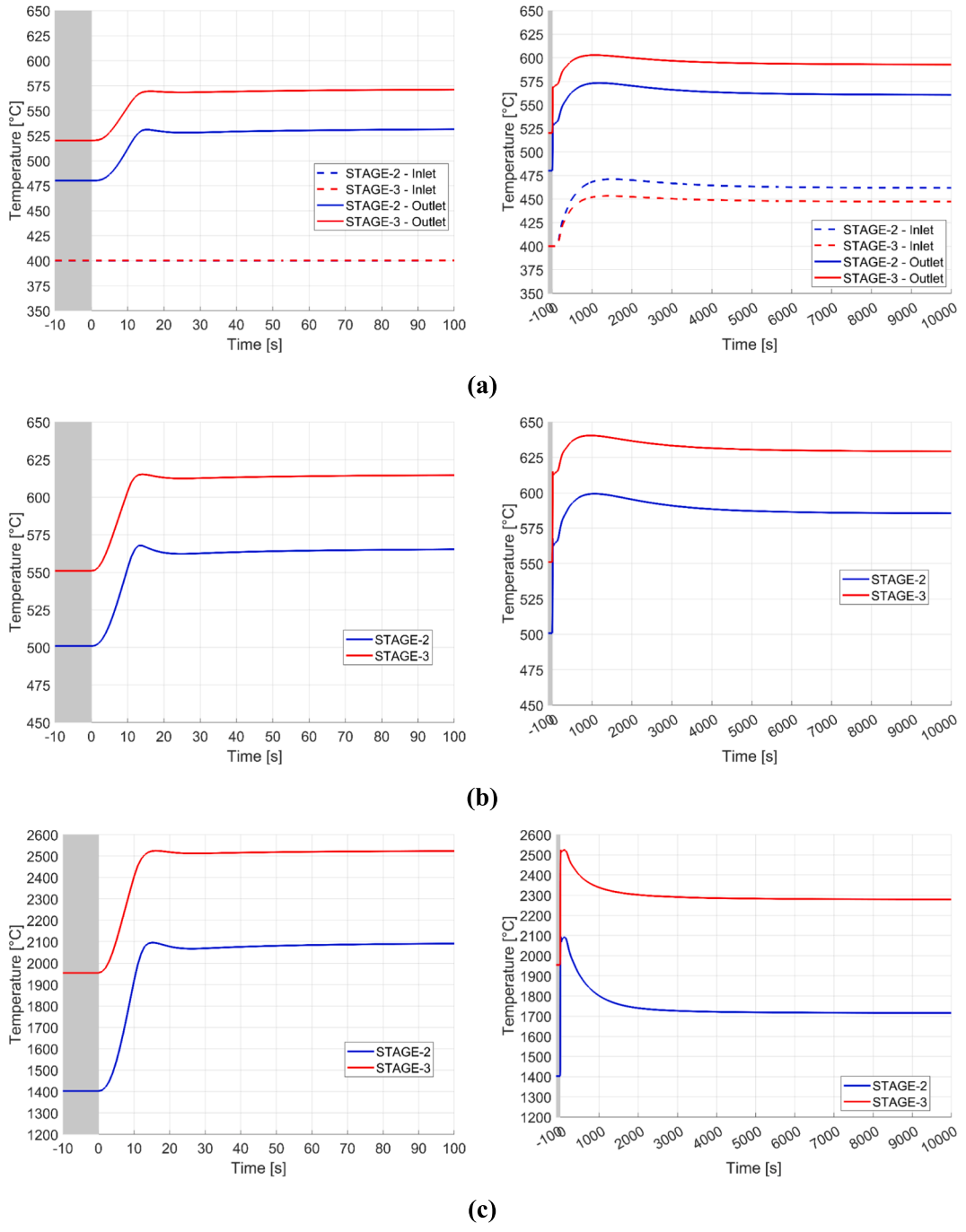

Fig. 10. UTOP transient: core inlet/outlet temperatures (a), maximum clad temperature (b) maximum fuel temperature (c), in short-term (left) and long-term (right).

forced circulation. The peak temperatures for both stages are about the 146 % of the nominal ones and the final values are 119 % (consistent with the core outlet temperature). Finally, of particular importance is to check the integrity of the second barrier (i.e., the clad). The clad integrity is preliminarily verified by the fact that the clad peak temperatures (which are 723 °C for STAGE 2 and 823 °C for STAGE 3) are lower than the melting point of 1417 °C, derived from (Luzzi, 2014). Therefore, there is no clad failure due to melting. Additionally, according to Eq. (8), the clad time-to-failure is estimated to be more than 2 years (875 days) for STAGE 2 and about 23 days for STAGE 3. The maximum fuel temperature evolution is depicted in Fig. 8c from which it can be seen that it follows the same trend as the power generated in the core. Therefore, as expected, no peaks are detected. For both stages, the final value is about 78 % of the nominal value (see Table 6 and Table 7).

4.3. *Unprotected transient overpower*

As far as the UTOP is concerned, the initiating event consists in an unforeseen reactivity insertion of 250 pcm in 10 s. The reactivity trend is assumed linear during the considered time window. The PIE features were selected according to the indications provided for this scenario in (Bandini and Polidori, 2013). Both the primary and secondary loops are assumed to remain in normal operation with no control of the corresponding mass flow rate. In this transient, no reactor SCRAM and no DHR intervention are postulated (they are assumed to fail). After PIE, the core relative power shows a maximum of 215 % and 172 % for respectively STAGE 2 and STAGE 3 (see Fig. 9a). As expect the peak occurs at the end of the insertion time window, i.e., 10 s after the start of transient. The magnitude of the relative power spike is different between

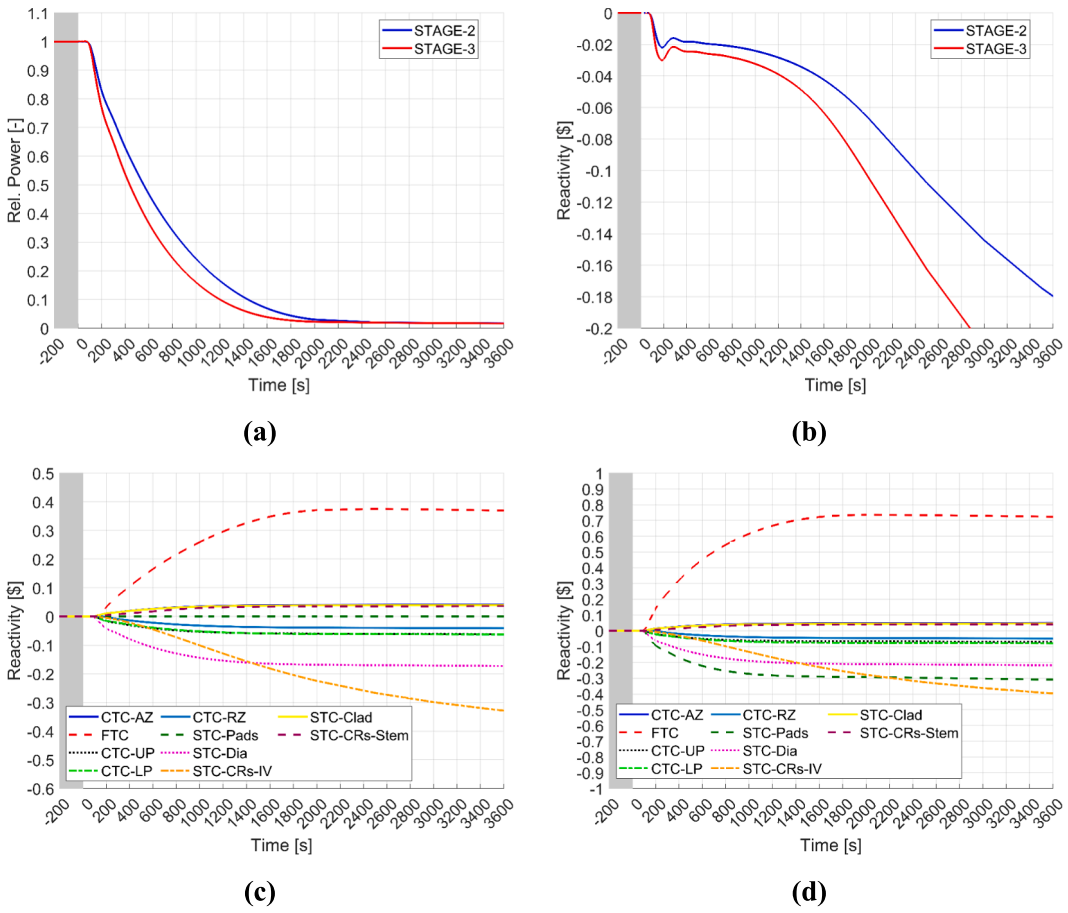

Fig. 11. ULOHS transient: relative reactor power (a), total reactivity (b), STAGE 2 (c) and STAGE 3 (d) NK feedbacks, in the short/mid-term.

the two stages. In STAGE 2, the relative extent of the power excursion is higher. This can be justified looking at Fig. 9c and Fig. 9d, gathering the NK feedbacks for STAGE 2 and STAGE 3, respectively. As visible, for STAGE 3 two main contributions counterbalance the positive reactivity insertion, i.e., FTC and STC-Pads (red and green dashed lines in Fig. 9d). Instead, for STAGE 2, the occurrence of the STC-Pads NK feedback is delayed (green dashed line in Fig. 9c), and this leads to a high relative power peak. Its initial absence is due to the logic implemented for this reactivity feedback, reflecting the physics behind this phenomenon, (see section 3). This NK feedback has a threshold effect based on the relative radial expansion between the pads (at core outlet) and the diagrid (at core inlet). In STAGE 3, the core nominal temperature level is higher and, consequently, the margin with respect to the temperature threshold that activates the STC-Pads feedback is reduced. Thus, a lower relative power excursion is needed to approach the limit. Instead, in STAGE 2, the rector works with lower temperature values and a higher relative power excursion is needed to activate the pads NK feedback. However, in both stages, the power spike is dampened in about 15 s. For both stages, a new equilibrium is reached in the mid-long term, characterized by a power level equals to 120 % of the nominal value. The reactor power trend is consistent with that of total reactivity, which is plotted in Fig. 9b. It can be noticed the maximum peak in the short term caused by the imposed positive reactivity insertion, which is then dampened in 15 s. The zero-value reactivity is restored in about 30 min. Regarding the different reactivity feedbacks, they are plotted in Fig. 9c and Fig. 9d for STAGE 2 and STAGE 3, respectively. As visible, in the short-term after PIE, the external reactivity insertion is mainly counterbalanced by the prompt negative FTC (red dashed line in Fig. 9c and Fig. 9d). Instead, in the mid-long term, the fuel temperatures decrease (see Fig. 10c), and the magnitude of the FTC lowers accordingly (with respect to the short-term peak value). However, the increase of the lead primary thermal cycle (see Fig. 10a) leads to the occurrence of other negative reactivity feedbacks, mainly the ones related to the IV axial expansion and the pads radial expansion (orange dotted-dashed line and green dashed line Fig. 9c and Fig. 9d, respectively). Together, these three contributions counterbalance the positive reactivity insertion.

The core inlet/outlet temperature evolutions are plotted in Fig. 10a. The core outlet temperature experiences two different surges. The first occurs in the short term and is related to the sudden reactivity insertion (first 10 s after PIE). The second is experienced in the mid-term when also the lower plenum temperature, i.e., the core inlet temperature starts to rise. This second one is smoother than the first one. The timing of this second increase depends on the thermal–hydraulic feedback provided by the steam generators. In the long term, i.e. after about 100 min, the core temperatures stabilize again. The primary average temperature increases of 71 °C and 60 °C for STAGE 2 and STAGE 3, respectively. In addition, in this new steady state characterizing the end of transient, the primary temperature difference corresponds to 99 °C and 146 °C for STAGE 2 and STAGE 3, corresponding to 123 % and 121 % of the nominal value (see Table 6 and Table 7). The increase in this parameter is due to the fact that the primary flow is kept constant during the overall transient. Thus, the power-to-flow ratio correspondingly increases. Referring to the maximum clad temperature (Fig. 10b), it follows the trend of the core outlet temperature. The peak temperature is reached at about 17 min in both stages and corresponds to 599 °C and 640 °C for STAGE 2 and STAGE 3, i.e., 120 % and 116 % of the nominal value in Table 6 and Table 7. These temperature levels are far below the melting point (Luzzi, 2014). In addition, according to Eq. (8), the time-to-failure is of 836 years and 101 years respectively for STAGE 2 and STAGE 3. Of course, if fuel and clad are into contact before the transient the ensuing

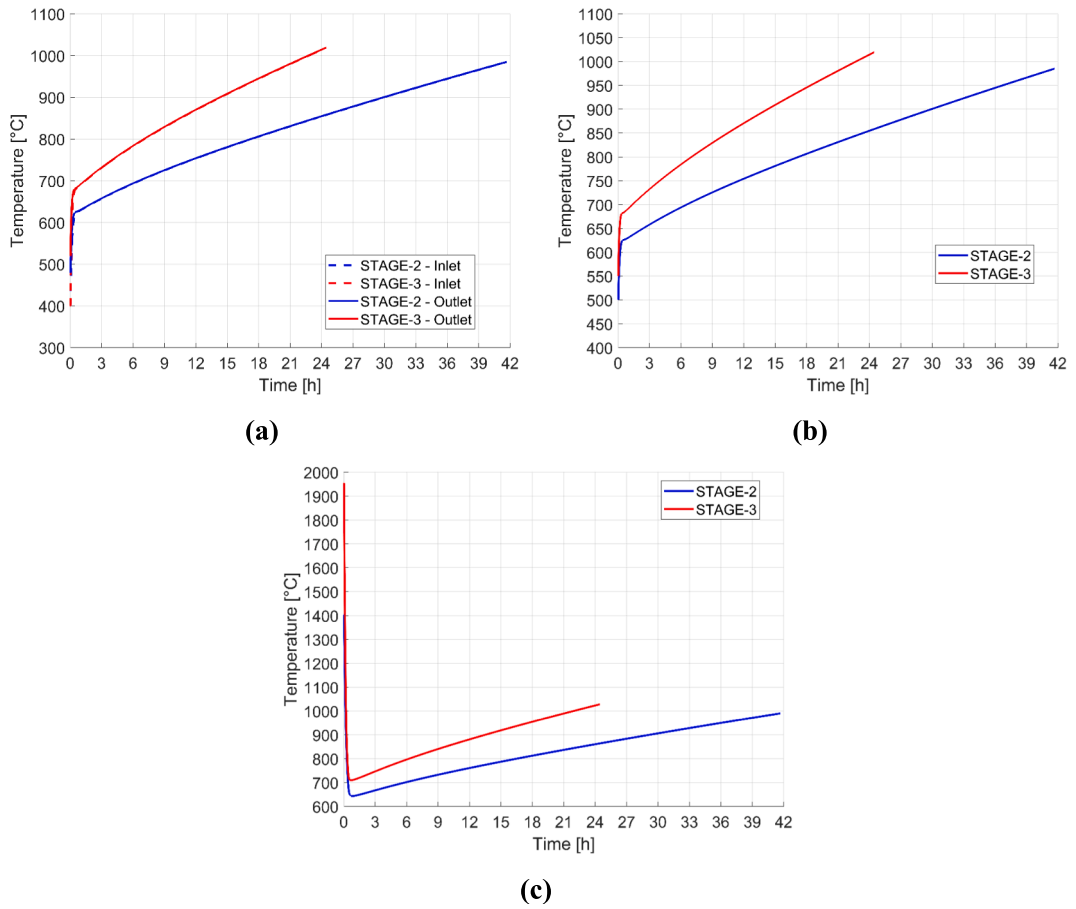

Fig. 12. ULOHS transient: core inlet/outlet temperatures (a), maximum clad temperature (b) maximum fuel temperature (c).

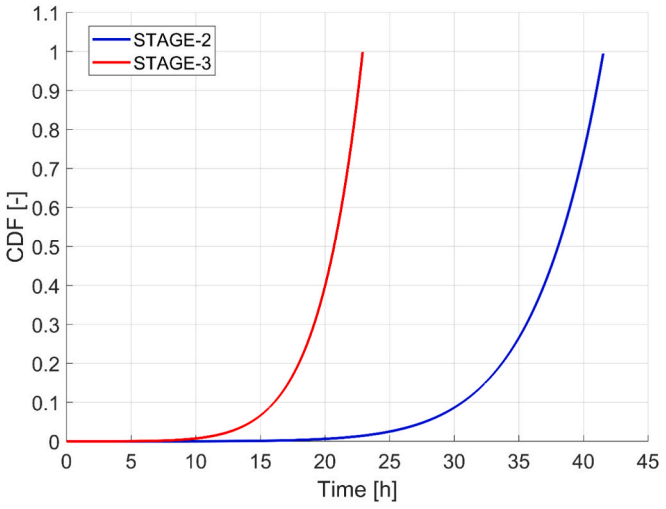

Fig. 13. ULOHS transient: time evolution of the clad CDF.

contact pressure could lead to clad failure due to plastic deformations rather than creep ones; notwithstanding the modest values reached by the clad temperature in this scenario, more detailed thermomechanical analysis should thus be performed to understand whether clad failure can occur and the corresponding driving mechanism. Finally, concerning the maximum fuel temperature, the trend for both stages is consistent with the reactor power evolution. After a sharp increase, a new equilibrium point is reached, higher than the nominal one. An important aspect to consider is the assessment of the integrity of the fuel itself. For this check, the maximum fuel temperature for both stages was compared to the melting temperature according to (Topliss, 1995). The maximum fuel temperature peak for STAGE 2 and STAGE 3 are respectively 2096 °C and 2525 °C. Given the isotopic composition of ALFRED fuel, indicated in (Grasso, 2019), the melting point is close to 2800 °C. Thus, in the case of a reactivity insertion whose magnitude approaches the prompt-criticality, no fuel melting occurs. However, the adopted trend (i.e., linear ramp in 10 s) is not the more conservative. In the future developments of the activity, other shapes will be considered and investigated.

4.4. *Unprotected loss of heat sink*

This transient is initiated by the simultaneous loss of all feedwater pumps. Also in this case, both SCRAM and DHR are supposed to fail. Instead, the primary loop is assumed to operate in normal operation with no control of the RCS mass flow rate. As discussed in section 3, the feedwater pumps are modelled by TMDPJUN 401 (see Fig. 5). This component allows the user to simulate any mass flow trend by providing the corresponding timetable. To model the secondary pump coast down the following equation was used, derived from (Argonne National Laboratory, 2019):

$$\overline{\Gamma} = \frac{t_{\frac{1}{2}}}{t + t_{\frac{1}{2}}} \tag{9}$$

Where:

- $\overline{\Gamma}$ is the relative mass flow rate, normalized with respect to the nominal value (see Table 6 and Table 7).
- t is the variable of time
- $t_{\frac{1}{2}}$ is the mass flow rate halving time which is set to 0.01 s

The halving time of the secondary flow rate was set based on typical feedwater pumps. For these components, the usual duration of the coast down transient swings from 1 to 5 s, according to the IAEA indications provided in (International Atomic Energy Agency., 1992). The accidental evolution was investigated without postulating the SGs isolation. Thus, the valves on the feedwater and steam lines are both open.

This accidental sequence is different from the two already discussed. Indeed, given the loss of the heat sink and the unprotected nature of the transient, the reactor experiences a persistent power unbalance. Due to the BCs associated with the scenario considered, the reactor cannot reach a new steady state configuration, as in the previous two cases. The power trend associated with the ULOHS is shown in Fig. 11a. The reactor power monotonically decreases towards the decay heat, that is the only source term still present after about 42 min. This is consistent with the trend of the total reactivity (Fig. 11b). It experiences a significant drop resulting in continuous negative reactivity feedback due to the system transient behaviour. This produces the shutdown of the fission reaction within the core. More in detail, the loss of the SGs and the unavailability of the DHR system cause an increase in the primary system temperatures. This provokes the occurrence of the corresponding negative reactivity feedbacks. The main contributes are the STCs (see Fig. 11c and Fig. 11d for STAGE2 and STAGE3, respectively). A deviation can be detected in Fig. 11 between the two stages. The difference is due to the lack in STAGE 2 of the STC-Pads NK feedback. This is because the FA radial pads are designed to be in contact at the STAGE 3 nominal conditions (see Table 1) and to introduce a negative reactivity feedback when experiencing a radial expansion greater than the one of the diagrid at the core inlet. During the ULOHS transient, both inlet and outlet core temperatures increase with a comparable slope due to the heating of the whole primary system. This consideration is valid for both the stages (see Fig. 12a). If STAGE 3 is considered, before the PIE occurrence, the pads are already in contact. Thus, during the accidental evolution, the core temperatures increase produces a relative radial expansion of these components and the occurrence of the corresponding NK feedback (green dashed line in Fig. 11d). Instead, when it comes to STAGE 2, the core nominal temperatures are lower, and the pads are not in contact before the PIE occurrence. For this, even if the core temperatures increase with the same slope of STAGE 3, this rise is not enough to produce the relative radial expansion needed to the pads to fill the gap (reminding that the diagrid is contemporarily expanding at the core inlet). Consequently, the STC-Pads is always zero (see green dashed line in Fig. 11c). Another aspect to be commented is related to the FTC. For both the stages, this contribute is initially positive due to the power decrease, resulting in a drop of the fuel temperature (see Fig. 12c). Then, in the mid-long term, this parameter restarts to rise due to the heating of the whole primary system. For this, the FTC inverts its trend and begins to decrease. At the end of transient, it is negative for both the calculations and, thus, contributes to the total negative reactivity. However, this aspect is irrelevant since in the long-term the only source term still active is the decay heat, that is unaffected by the NK feedbacks.

As depicted in Fig. 12a, due to the reduction of the reactor power the lead temperature difference across the core becomes negligible. For the same reason, clad (Fig. 12b) and fuel (Fig. 12c) temperatures approach the coolant ones. For what concerns the lead and clad temperatures, the main effect is the loss of the heat sink (i.e., both the SGs and the DHR system) and the consequent heating of the whole primary system. For this, the associated time trends monotonically rise. Instead, referring to the fuel temperature, it initially drops due to the reactor shutdown. Once approached the other system temperatures, i.e., coolant and clad, it experiences the same heating. Nevertheless, for the whole simulation time considered for the two cases (i.e., the grace time related to the clad CDF), this parameter keeps well below its nominal value.

As shown before, the SGs cannot remove the long-term thermal power generated within the core due to the decay heat, and the DHR system is not available as postulated in this transient. Thus, the primary system average temperature constantly increases. For this accident, to evaluate the thermal creep behavior of the cladding steel, a Cumulative Damage Function (CDF) approach has been adopted. This is a widely spread and validated criterion to assess the steel failure (Waltar et al., 2011). The CDF can be defined as follows:

$$\mathrm{CDF} = \sum_i \frac{\Delta t_i}{t_{R,i}} \tag{10}$$

Where:

- Δt_i is the simulation time-step.
- $t_{R,i}$ is the rupture time (calculated with Eq. (8).

The reactor grace time related to this accident was preliminarily defined as the time required for the CDF to reach the unity. As already said, $t_{R,i}$ was computed with Eq. (8), where the maximum cladding temperature (shown in Fig. 12b) was used. With this methodology, the reactor grace time is equal to approximately 42 h for STAGE 2 and 23 h for STAGE 3. The calculations were stopped when the simulation time approaches these values. The time evolution of the CDF is shown in Fig. 13. For both cases, the CDF profile has an exponential trend. In addition, the one of STAGE 3 shows a steeper slope, due to the higher temperatures characterizing this scenario.

5. Conclusions

This study presents a detailed numerical investigation of ALFRED's behaviour under three unprotected transient scenarios: Unprotected Loss of Flow, Unprotected Transient of Over-Power and Unprotected Loss of Heat Sink. By employing the RELAP5/Mod3.3 thermal–hydraulic system code, a preliminary assessment of ALFRED's response under these accidental conditions has been conducted, providing insights into its safety characteristics and dynamic performance. Preliminary results suggest that ALFRED may exhibit inherent safety features, but a more comprehensive analysis and validation with experimental data and facilities are required.

In the ULOF scenario, the loss of primary flow led to a gradual increase of the thermal field in the primary loop and the reactor reaches a new equilibrium point in about 15 min. In addition, the clad integrity has been preliminarily verified according to the selected safety criteria. Indeed, the maximum peak temperature is below the melting temperature and the time-to-failure preliminarily calculated is more than three months for both stages.

The UTOP scenario demonstrated the reactor's response to an inadvertent reactivity insertion, thanks to the critical role of feedback effects in counteracting power excursions and maintaining reactivity stability. A new equilibrium point is reached in about 17 min. Although a reactivity insertion is near to prompt-criticality, the integrity of the first two barriers is ensured. The maximum peak temperature of both clad and fuel are below to their respective melting point. Moreover, the clad time-to-failure preliminarily calculated largely exceeds intended reactor lifetime for both stages.

It should be noted that these are preliminary assessments that only refer to the clad, while a comprehensive analysis must also account for other failure possibilities, considering the thermomechanical loads on both the internal structures and the reactor vessel.

The main objective of the ULOHS transient is the assessment of the reactor grace time, as the absence of an effective heat sink resulted in a continuous temperature rise and no equilibrium is reached. The approach adopted to evaluate this parameter was based on the definition

of a CDF for the clad. According to this methodology, the computed grace time was equals to 36 h and 20 h for STAGE 2 and STAGE 3, respectively.

Finally, it is important to remind that heat losses have not been modelled—preventing an accurate assessment of the primary coolant's freezing margin. However, this phenomenon is expected to be a second order effect that does not jeopardize the reactor performances during the accidental conditions investigated in this study.

These findings contribute to the ongoing research efforts aimed at assessing the effectiveness of the current ALFRED reactor design, also providing valuable inputs for future uncertainty quantification and experimental validation. The present study highlights the need for more advanced numerical investigations to comprehensively assess the performance of the ALFRED reactor under accidental conditions, with particular attention to the coupling between neutronics and thermal-hydraulics during transients. Given that a 0-D point kinetics model was adopted in this work, the development of high-fidelity multiphysics models will be essential to capture localized phenomena and improve the predictive accuracy of the simulations. Future work will focus on extending the current numerical framework to address existing limitations, including the implementation of more detailed neutronic-thermal–hydraulic coupling, thermo-mechanical analyses, and the integration of sensitivity and uncertainty quantification methodologies. In parallel, code validation and benchmarking will be fundamental to ensure the reliability of the results and support the development of ALFRED reactor design.

CRediT authorship contribution statement

G. Khalil Youssef: Writing – original draft, Software, Methodology, Investigation, Formal analysis, Conceptualization. **C. Ciurluini:** Writing – original draft, Supervision, Methodology, Investigation, Conceptualization. **M. Caramello:** Writing – review & editing, Supervision, Methodology, Conceptualization. **F. Lodi:** Writing – review & editing, Supervision, Investigation, Formal analysis. **F. Giannetti:** Writing – review & editing, Supervision, Methodology, Conceptualization.

Declaration of competing interest

The authors declare that they have no known competing financial interests or personal relationships that could have appeared to influence the work reported in this paper.

Data availability

No data was used for the research described in the article.

References

GEN Iv International Forum, 2014. *Technology roadmap update for generation IV nuclear energy systems*. Retrieved March 13, 2025, from. https://www.gen-4.org/gif/upload/docs/application/pdf/2014-03/gif-tru2014.pdf.

Cinotti, L., et al., (2009). *Lead-cooled fast reactor (LFR): Overview and perspectives* (pp. 174–181). Organisation for Economic Co-operation and Development – Nuclear Energy Agency, Committee on the Safety of Nuclear Installations (OECD/NEA/CSNI), Le Seine Saint-Germain, 12 boulevard des Iles, F-92130 Issy-les-Moulineaux, France.

International Atomic Energy Agency (2025), "Analysis and Modelling of Severe Accidents for Liquid Metal Fast Reactors," IAEA-TECDOC-2079.

Alemberti, A., et al., (2017). *Status of generation–IV lead fast reactor activities*. In *International Conference on Fast Reactors and Related Fuel Cycles: Next Generation Nuclear Systems for Sustainable Development (FR17)* (p. 10). Retrieved January 9, 2025, from https://inis.iaea.org/records/rbzxp-qrw68.

Orlov, V.V., et al., 2005. The closed on–site fuel cycle of the Brest reactors. Progress in Nuclear Energy 47 (1–4), 171–177. https://doi.org/10.1016/j.pnucene.2005.05.017.

Baeten, P., Schyns, M., Fernandez, R., De Bruyn, D., Van den Eynde, G., 2014. MYRRHA: a multipurpose nuclear research facility. EPJ Web of Conferences 79, 03001. https://doi.org/10.1051/epjconf/20137903001.

Bogdán Yamaji, Graham Kennedy, Guy Scheveneels, Tewfik Hamidouche. *MYRRHA reference design and initiation events.* European Project ANSELMUS, Deliverable 1.3.

Sekimoto, H., et al., (2000). A new reactor burnup concept CANDLE. In *PHYSOR* (Pittsburgh, PA).

Sekimoto, H., & Nagata, A. (2008). *Fuel cycle for "CANDLE" reactors*. Paper presented at the Workshop on Advanced Reactors With Innovative Fuels (ARWIF-2008), Tsuruga/Fukui, Japan.

Sekimoto, H., Ryu, K., Yoshimura, Y., 2001. CANDLE: the New Burnup Strategy. Nucl. Sci. Engin. 139, 306–317.

Gao, Y., Takahashi, M., Cavallotti, C., Raos, G., 2018. Molecular dynamics simulation of metallic impurity diffusion in liquid lead-bismuth eutectic (LBE). Journal of Nuclear Materials 501, 253–260. https://doi.org/10.1016/j.jnucmat.2018.01.044.

Martinelli, L., Courouau, J.-L., Balbaud-Célérier, F., 2011. Oxidation of steels in liquid lead bismuth: Oxygen control to achieve efficient corrosion protection. Nuclear Engineering and Design 241 (5), 1288–1294. https://doi.org/10.1016/j.nucengdes.2010.07.039.

Smith, C.F., et al., 2008. SSTAR: the US lead–cooled fast reactor (LFR). Journal of Nuclear Materials 376 (3), 255–259. https://doi.org/10.1016/j.jnucmat.2008.02.049.

Greenspan, E., 2002. The encapsulated nuclear heat source reactor for low–waste proliferation–resistant nuclear energy. Progress in Nuclear Energy 40 (3–4), 431–439. https://doi.org/10.1016/S0149-1970(02)00035-5.

P. Ferroni et al. The Westinghouse Lead Fast Reactor: Design Overview and Update on Development Activities 2022 Vienna, Austria.

Choi, S., et al., (2011). URANUS: Korean lead–bismuth cooled small modular fast reactor activities. In *ASME 2011 Small Modular Reactors Symposium (SMR 2011)*. doi: 10.1115/SMR2011-6650.

Dong, S., et al., 2025. Development and application of three-dimensional multi-physics and multi-scale coupling program for lead-cooled fast reactor. Annals of Nuclear Energy 219, 111486. https://doi.org/10.1016/j.anucene.2025.111486.

Luo, Y., et al., 2022. Neutronic analysis of the unfolding process of the LOTUS reactor design. Annals of Nuclear Energy 173, 109102. https://doi.org/10.1016/j.anucene.2022.109102.

Luo, Y., et al., 2025. Neutronic and thermal-hydraulic coupling analysis of the dynamic unfolding process of the LOTUS reactor. Nuclear Engineering and Design 432, 113798. https://doi.org/10.1016/j.nucengdes.2024.113798.

M. Frignani et al. ALFRED: a Strategic Vision for LFR Deployment, ANS Winter meeting 2017 2017 Washington D.C.

U.S. Nuclear Regulatory Commission. (1989). *Quantifying reactor safety margins: Application of code scaling, applicability, and uncertainty evaluation methodology to a large–break loss–of–coolant accident* (NUREG/CR–5249). Retrieved February 10, 2025, from https://www.nrc.gov/docs/ML0303/ML030380473.pdf.

Liao, J., et al., 2021. Development of phenomena identification and ranking table for Westinghouse lead fast reactor's safety. Progress in Nuclear Energy 131, 103577. https://doi.org/10.1016/j.pnucene.2020.103577.

CORDIS. (n.d.). Project ID 101061185. Retrieved from https://cordis.europa.eu/project/id/101061185.

Grasso, G., et al., 2018. Stress–testing the ALFRED design – Part I: Impact of nuclear data uncertainties on design extension conditions transients. Progress in Nuclear Energy 106, 372–386. https://doi.org/10.1016/j.pnucene.2018.03.013.

Nuclear Safety Analysis Division. (2003). *RELAP5/MOD3.3 Code Manual Volume I: Code structure, system models, and solution methods*. Information Systems Laboratories, Inc. (Rockville, MD; Idaho Falls, ID).

Frignani, M., et al., 2019. ALFRED staged approach. Proceedings of the ICAPP 2019 Conference.

Alemberti, A., et al., 2020. ALFRED reactor coolant system design. Nuclear Engineering and Design 370, 110884. https://doi.org/10.1016/j.nucengdes.2020.110884.

Grasso, G., et al., 2014. The core design of ALFRED, a demonstrator for the European lead-cooled reactors. Nuclear Engineering and Design 278, 287–301. https://doi.org/10.1016/j.nucengdes.2014.07.032.

Grasso, G., et al., 2019. May). an improved design for the ALFRED core. Paper presented at the *International Congress on advances in Nuclear Power Plants*. Juan–les–Pins, France.

Petrovich, C., et al., 2013. Definition of the ETDR core and neutronic characterization (Lead-cooled European Advanced DEmonstration Reactor – LEADER. Technical Report).

Caramello, M., et al., 2017. Thermal–hydraulic analysis of a passively controlled DHR system. Progress in Nuclear Engineering 99, 127–139. https://doi.org/10.1016/j.pnucene.2017.05.015.

Frignani, M., et al., 2019. ALFRED: a revised concept to improve pool–related thermal–hydraulics. Nuclear Engineering and Design 355, 110359. https://doi.org/10.1016/j.nucengdes.2019.110359.

OECD/NEA Nuclear Science Committee, 2015. *Handbook on lead–bismuth eutectic alloy and lead properties, materials compatibility, edition, thermal–hydraulics and technologies*. Retrieved January 20, 2025, from. https://www.oecd-nea.org/jcms/pl_14972/handbook-on-lead-bismuth-eutectic-alloy-and-lead-properties-materials-compatibility-thermal-hydraulics-and-technologies-2015-edition?details=true.

Tarantino, M., et al., 2012. Post Test Analysis of ICE Tests Vol. 2, 703–712.

Forgione, N., et al., 2019. Post–test simulations for the NACIE–UP benchmark by STH codes. Nuclear Engineering and Design 353, 110279. https://doi.org/10.1016/j.nucengdes.2019.110279.

Information Systems Laboratories, Inc. (2006). *RELAP5/MOD3.3 code manual. Volume V: User's guidelines*. Nuclear Safety Analysis Division. Prepared for the U.S. Nuclear Regulatory Commission, Division of Systems Research, Office of Nuclear Regulatory Research.

International Atomic Energy Agency, 2008. *Thermophysical properties of materials for nuclear engineering: a tutorial and collection of data*. Retrieved February 26, 2025, from https://www-pub.iaea.org/MTCD/Publications/PDF/IAEA-THPH_web.pdf. IAEA.

Luzzi, L., et al., 2014. *Modeling and analysis of nuclear fuel pin behavior for innovative lead cooled FBR* [Technical Report]. ENEA.

Arp, V. D., et al., (1998). Thermophysical properties of helium–4 from 0.8 to 1500 K with pressures to 2000 MPa (Revised) (NIST Tech. Note 1334). National Institute of Standards and Technology. Retrieved January 14, 2025, from https://nvlpubs.nist.gov/nistpubs/Legacy/TN/nbstechnicalnote1334.pdf.

American Nuclear Society, ANSI/ANS-5.1-1994, Decay Heat Power in Light Water Reactors, August 23, 1994.

Brown, D.A., et al., 2018. ENDF/B-VIII.0: the 8th Major Release of the Nuclear Reaction Data Library with CIELO-project Cross Sections, New Standards and thermal Scattering Data. Nuclear Data Sheets 148, 1–142. https://doi.org/10.1016/j.nds.2018.02.001.

Castelluccio, D., et al., 2022. Realisation of an adjusted nuclear data library based on ENDF/B-VIII.0 nuclear data evaluations for the ALFRED core. In FR-22 Proceedings.

Kim, C. S. *Thermophysical properties of stainless steel.* Argonne National Laboratory. (Prepared for the U.S. Energy Research and Development Administration).

Mikityuk, K., 2009. Heat transfer to liquid metal: Review of data and correlations for tube bundles. Nuclear Engineering and Design 239 (4), 680–687. https://doi.org/10.1016/j.nucengdes.2008.12.014.

The US Nuclear Regulatory Commission (2006), RELAP5/MOD3.3 code manual volume 4, Models and Correlations, NUREG/CR-5535; USNRC: Washington, DC, USA.

Dittus F. W. and Boelter L. M. K (1930). Heat Transfer in Automobile Radiators of the Tubular Type. *Publications in Engineering*, 2, 443-461. University of California, Berkeley.

Inayatov, A.Y., 1975. Correlation of Data on Heat transfer Flow Parallel to Tube Bundles at Relative Tube Pitches of 1.1 < s/d < 1.6. Heat Transfer-Soviet Research 7, 3, 84–88.

Chen, J.C., 1966. A Correlation for Boiling Heat transfer to Saturated Fluids in Convective Flow. Process Design and Development 5, 322–327. https://doi.org/10.2172/4636495.

Groeneveld, D.C., 1986. 1986 AECL-UO critical Heat Flux Lookup Table. Heat Transfer Engineering 7 (1–2), 46–62. https://doi.org/10.1080/01457638608939644.

Chen J. C., Sundaram R. K., and Ozkaynak F. T. (1977). A Phenomenological Correlation for Post-CHF Heat Transfer. NUREG-0237.

Bromley, L.A., 1950. Heat transfer in Stable Film Boiling. Chemical Engineering Progress 46, 221–227.

Sudo, Y., 1980. Film Boiling Heat transfer during Reflood phase in Postulated PWR Loss-of-Coolant Accident. Journal of Nuclear Science and Technology 17 (7), 516–530.

Colebrook, C. F., & White, C. M. (1937). Experiments with fluid friction in roughened pipes. *Proceedings of the Royal Society of London. Series A, Mathematical and Physical Sciences, 161*(906), 367–381.

Lockhart, R.W., Martinelli, R.C., 1949. Proposed Correlation of Data for Isothermal Two-phase, Two-Component Flow in Pipes. Chemical Engineering Progress 45 (1), 39–48.

Idelchik, I.E., 1986. *Handbook of hydraulic resistance*, (2nd ed.). Hemisphere Publishing Corporation.

Bandini, G., & Polidori, M. (2013). Report on the results of analysis of DEC events for the ETDR (ALFRED) (ENEA–EU Contract, Deliverable DEL022, LEADER Project, EU 7th Framework Programme, Grant Agreement No. FP7–249668). Retrieved February 14, 2025, from https://iris.enea.it/bitstream/20.500.12079/7519/1/UTFISSM-P9SZ-007.pdf.

Samanta, P., et al. (2019, June). *NRC regulatory history of non-light water reactors (1950–2019)*. doi:10.2172/1579511.

Topliss, J.R., et al., 1995. July). Measurement and Analysis of MOX Physical Properties. United Kingdom), Newby Bridge, Windermere.

Lodi, F., Grasso, G., 2018. Stress–testing the ALFRED design – Part III: Safety margins evaluation. Progress in Nuclear Energy 106, 433–439. https://doi.org/10.1016/j.pnucene.2018.04.003.

Lodi, F., 2018. Engineering the fuel Pin Thermo-mechanic Code TEMIDE: Validation and Application. ENEA Technical Report. XSRS-P000–001.

Argonne National Laboratory, 2019. April 26). Analysis of VTR primary pump coastdown [Technical Report]. Nuclear Science and Engineering Division.

International Atomic Energy Agency. (1992). *Procedures for conducting probabilistic safety assessments of nuclear power plants (Level 1)* (Safety Series No. 50–P–4). IAEA. Retrieved January 21, 2025, from https://www.iaea.org/publications/3759/procedures-for-conducting-probabilistic-safety-assessments-of-nuclear-power-plants-level-1.

Waltar, A.E., Todd, D.R., Tsvetkov, P.V. (Eds.), 2011. Fast Spectrum Reactors. Springer, New York.